CCFE-PR(16)62

K.G. McClements and E.D. Fredrickson

Energetic particles in spherical tokamak plasmas

Energetic particles in spherical tokamak plasmas

K.G. McClements[1] and E.D. Fredrickson[2]

[1]CCFE, Culham Science Centre, Abingdon, Oxfordshire OX14 3DB, UK
[2]Princeton Plasma Physics Laboratory, Princeton, New Jersey 08543, USA

Energetic particles in spherical tokamak plasmas

K.G. McClements[1] **and E.D. Fredrickson**[2]

[1] CCFE, Culham Science Centre, Abingdon, Oxfordshire OX14 3DB, UK
[2] Princeton Plasma Physics Laboratory, Princeton, New Jersey 08543, USA

Abstract

Spherical tokamaks (STs) typically have lower magnetic fields than conventional tokamaks, but similar mass densities. Suprathermal ions with relatively modest energies, in particular beam-injected ions, consequently have speeds close to or exceeding the Alfvén velocity, and can therefore excite a range of Alfvénic instabilities. STs heated with neutral beams, such as the Mega Amp Spherical Tokamak (MAST) and the National Spherical Torus Experiment (NSTX), have thus provided an opportunity to study toroidal Alfvén eigenmodes (TAEs), together with higher frequency global Alfvén eigenmodes (GAEs) and compressional Alfvén eigenmodes (CAEs), which could affect beam current drive and channel fast ion energy into bulk ions in future devices. In NSTX GAEs were correlated with a degradation of core electron energy confinement. In MAST pulses with reduced magnetic field, CAEs were excited across a wide range of frequencies, extending to the ion cyclotron range, but were suppressed when hydrogen was introduced to the deuterium plasma, apparently due to mode conversion at ion-ion hybrid resonances. At lower frequencies fishbone instabilities caused fast particle redistribution in some MAST and NSTX pulses, but this could be avoided by moving the neutral beam line away from the magnetic axis or by operating the plasma at either high density or elevated safety factor. Fast ion redistribution has been observed during GAE avalanches on NSTX, while in both NSTX and MAST fast ions were transported by saturated kink modes with toroidal mode number $n = 1$, sawtooth crashes, resonant magnetic perturbations and TAEs. High energy charged fusion products are unconfined in present-day STs, but have been shown in MAST to provide a useful diagnostic of beam ion behaviour, supplementing the information provided by neutron detectors. In MAST electrons were accelerated to highly suprathermal energies as a result of edge localised modes, while in both MAST and NSTX ions were accelerated due to internal reconnection events. Ion acceleration has also been observed during merging-compression start-up. Finite Larmor radius effects often cannot be neglected in the theoretical description of fast ions in STs due to the relatively low magnetic field. Also the restriction of many kinetic codes to modes in the sub-cyclotron range means that they cannot be used to model the highest frequency CAEs observed in MAST and NSTX. The resulting severe demands placed on the modelling of energetic particles in existing STs will apply also to future ST reactors, since fusion alpha-particles in such devices will have orbits similar to those of beam ions in MAST and NSTX.

Keywords: spherical tokamak, fast ion transport, Alfvén eigenmodes, fishbones

1 Introduction

The ultimate success of deuterium-tritium fusion as a large-scale energy source relies on highly suprathermal fusion α-particles being confined (magnetically or inertially) for long enough to maintain the fuel plasma at thermonuclear temperatures. Spherical tokamaks (STs), which represent one possible route to a fusion reactor via magnetic confinement [1], are characterised by relatively low magnetic fields, with the result that not only charged fusion products but also the lower energy beam ions commonly used for auxiliary plasma heating are typically super-Alfvénic in such devices. STs are thus particularly susceptible to Alfvénic instabilities driven by energetic ions. The use of low magnetic fields in STs also means that energetic ions have relatively large Larmor radii relative to the machine size, with the consequence that guiding centre theory often does not provide an adequate description of the particle dynamics.

This is a Topical Review of recent developments in the experimental and theoretical study of energetic particles in spherical tokamaks, focussing almost exclusively on the two largest devices of this type in the world, the Mega Amp Spherical Tokamak (MAST) at the Culham Science Centre in the UK and the National Spherical Torus eXperiment (NSTX) at Princeton Plasma Physics Laboratory in the USA. After a discussion in section 2 of the diagnostics used in STs to study energetic particles and the instabilities driven by them, we review recent work on fast particle-driven Alfvén eigenmodes (section 3) and kink modes (section 4), and then discuss the redistribution of fast ions in STs due to non-resonant magnetohydrodynamic (MHD) instabilities (section 5) and static perturbations to the otherwise two-dimensional ST equilibrium magnetic field (section 6). The production of energetic particles (both ions and electrons) as a result of plasma processes rather than auxiliary heating or fusion reactions is considered in section 7, and we end with a brief discussion of prospects for energetic particle studies in upgraded versions of MAST and NSTX (section 8).

2 Diagnostics of fast ions and fast ion-driven instabilities in STs

2.1 Neutron detectors

Since the fuel species in the two large STs (MAST and NSTX) was usually deuterium, neutron production generally occurred via one of the two main branches of the deuterium-deuterium fusion reaction:

$$\mathrm{D} + \mathrm{D} \rightarrow {}^{3}\mathrm{He}(0.82\mathrm{MeV}) + \mathrm{n}(2.45\mathrm{MeV}). \quad (1)$$

Plasmas in both MAST and NSTX were heated with deuterium neutral beams at power levels of several MW and with primary injection energies that were variable but always in the tens of keV range, while the core plasma temperatures were generally around 1 keV. Since the DD fusion cross-section is a strongly-increasing function of deuteron energy in the 1-100 keV range [2], only a small fraction of the neutrons were thermonuclear (typically fewer than 1%) [3]; many more were produced by reactions

between energetic beam ions and other beam ions ("beam-beam"), and the greatest number resulted from reactions between beam ions and bulk ions ("beam-thermal"). As a result, the flux of neutrons resulting from fusion reactions in the plasma provided a simple and very useful measure of fast ion confinement.

The neutron rate can be reduced due to fast ion losses or redistribution of fast ions to regions of lower bulk deuterium or beam ion density, or lower bulk deuterium temperature. Another important point is that fast ions can lose energy by driving instabilities, such as toroidal Alfvén eigenmodes (TAEs), and that loss of energy can itself contribute significantly to a reduction in the neutron rate. It is important to be able to discriminate between changes in neutron flux due to particle losses and those due to redistribution by making spatially-resolved measurements of the neutron flux in addition to the total flux. Liquid scintillator detectors were used in a prototype neutron camera on MAST, with four lines of sight, making it possible to measure changes in the emission profile with a time resolution of about 1 ms [4], while changes in the total neutron flux could be measured with higher time resolution (10 μs) using a ^{235}U fission chamber [5].

2.2 Charged fusion product detectors

As an alternative to neutron detection, it is possible to use the charged products of the other main deuterium-deuterium fusion reaction

$$\mathrm{D} + \mathrm{D} \rightarrow \mathrm{T}(1.0\mathrm{MeV}) + \mathrm{p}(3.0\mathrm{MeV}), \tag{2}$$

as a diagnostic of deuterium fast ions in ST plasmas. The toroidal magnetic field in MAST was typically about 0.4 T, which meant that 3.0 MeV protons and 1.0 MeV tritons had Larmor radii ρ of up to about 60 cm, comparable to the plasma minor radius. The orbit widths of passing particles are approximately equal to $q\rho$ where $q \sim 1$ is the plasma safety factor (defined as the number of toroidal circuits made by a magnetic field line in one poloidal circuit) and ρ is evaluated using the full velocity rather than its perpendicular component, and the orbit widths of trapped particles are invariably higher than those of passing particles at the same energy. It is thus apparent that essentially all of the fusion protons and tritons produced in MAST were lost promptly from the plasma. Their detection could be used to infer information on the beam ion distribution similar to that provided by neutron diagnostics. A prototype 4-channel charged fusion product detector was used in the last MAST campaign [6]; results obtained using this diagnostic will be discussed in section 5.

Fusion protons and tritons can in principle be detected with higher efficiency (and hence better Poisson statistics) than neutrons, since any energetic charged particle passing through a suitable detector produces a measurable voltage signal, whereas most neutrons generally pass through detectors (whether of the scintillator or fission chamber type) without being recorded. On the other hand measurements of charged fusion products are more complicated to interpret than measurements of neutrons, for the obvious reason that the former gyrate in the ST magnetic field whereas the latter do not.

2.3 Neutral particle analysers

Neutral particle analysers (NPAs) measure fluxes of hydrogen and deuterium neutral atoms produced by charge exchange between high energy ions and either beam neutrals or low energy neutrals; they are used to measure the energy distributions of thermal and energetic ions [7, 8]. MAST and NSTX were equipped with NPAs in which charge-exchanged neutrals leaving the plasma were ionized in a stripping cell and then dispersed according to their mass and energy by parallel electric and magnetic fields produced by D-shaped magnets and electrostatic deflection systems. The NPA diagnostic on NSTX was steerable between shots, making it possible to scan the tangency radius of the NPA sightline. Much smaller solid-state NPAs (ssNPA), based on diamond or silicon photodiodes, have also been used on NSTX. These are smaller, cheaper, thus can more easily have multiple sightlines and are more easily installed on the machine, but have poorer energy resolution (particle energy is determined by pulse height analysis).

2.4 Fast ion deuterium-alpha spectrometry

An energetic beam deuterium ion can capture an electron from a beam or thermal neutral atom of the same species, creating an excited atomic state with principal quantum number $n = 3$ which de-excites to an $n = 2$ state via the emission of a deuterium-alpha (Dα) photon. When detected, this light is Doppler-shifted from the Dα rest wavelength of 656.1nm by an amount determined by the line-of-sight velocity of the original deuterium ion. A fast ion deuterium-alpha (FIDA) spectrometer can thus be used to measure the evolving velocity distribution of fast ions present in the emitting region, which is defined by the intersection of the beamline and the FIDA line-of-sight when the neutralising electron is provided by a beam neutral. If a range of FIDA lines-of-sight is available, spatial information on the fast ion distribution can also be obtained. FIDA systems were used on both NSTX [9] and MAST [10].

2.5 Fast ion loss detectors

The detection of fast particle losses from tokamak plasmas provides a very useful measure of non-classical transport arising from instabilities or three-dimensional magnetic field perturbations. A common method of detecting such losses, which was implemented on NSTX [11] and will be used on the upgraded version of MAST, is based on the detection of light resulting from the impact of fast ions on a scintillator plate lying just outside the plasma. Fast ions passing through an aperture onto the plate are dispersed in energy and pitch angle by the plasma's own magnetic field, so that the velocity space dependence of the losses can be studied.

2.6 Magnetic coils

As discussed in section 1, the use of low toroidal fields means that Alfvénic instabilities occur frequently in STs, and Alfvénic modes have been detected in MAST and NSTX at frequencies of up to several MHz. Mirnov coils provide the primary method of

detecting these modes, and by comparing the phases of signals recorded in coils at different toroidal locations it is possible to determine the toroidal mode number n [1]. Using the Outboard Mirnov Array for High frequency data Acquisition (OMAHA) array on MAST it was also possible to measure all three components of the fluctuating magnetic field, and hence determine the mode polarization, up to a maximum frequency of 5 MHz [12].

The fast toroidal Mirnov array on NSTX was built with coils oriented to measure the vertical (poloidal) and toroidal magnetic fluctuations (the recorded magnetic fluctuations had no radial component since the coils were mounted on the vacuum vessel wall). This coil array was used to measure the polarization of magnetic fluctuations, and it was found that the highest frequency magnetic fluctuations had compressional polarization, at least at the plasma edge, leading to their identification as compressional Alfvén eigenmodes (CAEs) [13].

2.7 Soft X-ray emission

Fast particle-driven modes can be detected using diagnostics other than magnetic coils. Typically these rely on the detection of radiation emitted inside the plasma, and as such they can in principle provide direct information on mode structure that cannot be obtained from coil data. One such diagnostic that has been successfully exploited in spherical tokamaks is soft X-ray emission. MAST was equipped with soft X-ray pinhole cameras which provided a total of 54 lines-of-sight, covering almost the entire plasma cross-section [14]. One set of lines-of-sight in the machine midplane provided a radial resolution of about 8 cm. NSTX was equipped with an ultra soft X-ray (USXR) detector array, with a sufficiently high sampling rate (190 kHz) for the detection of some fast particle-driven instabilities [15].

2.8 Reflectometers

Plasmas reflect electromagnetic radiation at frequencies below the electron plasma frequency, which is density-dependent. For typical plasma densities, the electron plasma frequency lies in the microwave range. Operating in much the same way as radar, a reflectometer system can be used to measure the distance to a specific density surface by determining the phase shift of reflected microwave radiation. Reflectometers have intrinsically high frequency bandwidth and good sensitivity. An array of reflectometers on NSTX has been used to measure the internal amplitude and structure of density fluctuations associated with a variety of fast particle-driven modes, including TAEs, global Alfvén eigenmodes (GAEs) and CAEs [16]. A variant of this technique, Doppler backscattering, was used in MAST primarily as a diagnostic of bulk ion-driven turbulence [17], but could also be used to detect CAEs, as in NSTX.

[1] Throughout this paper we adopt the convention that a mode propagating in the positive φ direction in (R, φ, Z) right-handed cylindrical coordinates has $n > 0$. In normal MAST and NSTX operation this was the plasma current direction.

2.9 Beam emission spectroscopy

In addition to the Dα light produced by deuterium beam ions that have captured electrons (which forms the basis of the FIDA diagnostic technique described above), this type of emission can also be produced by neutral beam atoms excited by collisions with electrons. Beam emission spectroscopy (BES) is based on the detection of Dα emission from collisionally-excited beam atoms. The radiated flux increases with electron density, so BES provides another method of measuring small amplitude, high frequency density fluctuations inside the plasma. However, the interpretation of BES measurements is complicated by "passive" FIDA light produced by beam ions redistributed towards the plasma boundary, where they charge-exchange with recycling neutrals [18].

3 Fast particle-driven Alfvén eigenmodes

As indicated previously, super-Alfvénic beam ions in MAST and NSTX provided strong drive for a wide range of Alfvénic instabilities. In this section we discuss experimental measurements and modelling of these instabilities.

3.1 Toroidal Alfvén eigenmodes

TAEs are weakly-damped or unstable modes which can exist inside the lowest-frequency (toroidicity-induced) gap in the otherwise continuous spectrum of strongly-damped waves arising from singularities in the shear Alfvén eigenmode equation. In the large aspect ratio limit the fractional width of the TAE gap is given by [19]

$$\frac{\Delta\omega}{\omega} \simeq \frac{3r}{2R}, \tag{3}$$

where R is tokamak major radius, r is minor radial distance from the magnetic axis and $\omega = \omega_{\mathrm{TAE}} \equiv c_A/2qR$, c_A being the Alfvén speed. Although this expression does not give an accurate value for the TAE gap width at tight aspect ratio ($r \sim R$), it shows qualitatively that TAE spectra in STs differ from those in conventional tokamaks, in that the toroidicity-induced gaps are much wider in the former than in the latter, with the result that TAEs can exist in a given equilibrium with a broader range of frequencies. Numerical calculations of continuous spectra and TAEs for equilibria in the Small Tight Aspect Ratio Tokamak (START) demonstrate this point [20]. Energetic ions in STs often have large orbit widths, as well as large Larmor radii; this has consequences for the toroidal mode numbers n of TAEs excited in these devices, since high n modes are generally more localised in minor radius and the wave-particle interaction becomes weaker when the particles spend only part of their drift orbit in the vicinity of the mode [21]. TAEs excited in MAST, for example, generally had $n = 1$ [22], although in NSTX the simultaneous excitation of TAEs with a range of n values ("TAE avalanches") was often observed [23]. The modelling of TAEs in STs is also complicated by the fact that plasmas in these devices often rotate toroidally with Mach numbers approaching unity

and can have strongly anisotropic pressure, which affects the Alfvén continuum and hence the TAE spectrum [24, 25].

TAEs have been observed in many conventional aspect ratio tokamaks when fast ions are present with velocities parallel to the magnetic field $v_\parallel$ exceeding c_A (or, in some circumstances, $c_A/3$). These modes have been found to be correlated with fast ion redistribution. Most commonly the fast ions exciting TAEs in conventional tokamaks are accelerated by radio-frequency waves; neutral beams in such devices are usually sub-Alfvénic, and thus cannot drive TAEs via the $v_\parallel = c_A$ resonance. These modes are frequently observed in STs, largely because ST plasmas have densities and neutral beam injection (NBI) energies that are similar to those in conventional tokamaks, but lower magnetic fields, with the result that beam ions at the full injection energy are usually super-Alfvénic. Fast ion redistribution correlated with TAEs is commonly observed in beam-heated ST plasmas [26]. Careful modelling of the effects of temporal variations in TAE amplitude, mode structure and frequency on fast particles (tracked using the `ORBIT` code) has yielded results that are in good agreement with experimentally-measured neutron rate drops [23]. A somewhat surprising result of these simulations is that around half of the measured neutron rate drops can be attributed to anomalous (non-collisional) slowing down of fast particles through interaction with the mode, rather than to loss or redistribution. As shown in figure 1, the average energy loss resulting from the interaction is quite small (5.4%), but the fusion reaction rate is a strongly increasing function of the particle energy. This result illustrates the important point that velocity transport as well as spatial transport may need to be considered in order to model accurately the interaction of energetic particles with some MHD modes; typically only spatial transport is included explicitly in the modelling of fast particle interactions with fishbones, for example [27].

A striking difference between TAEs in STs and those in conventional tokamaks is that the former typically exhibit strong, fast frequency chirps. These chirps can take the mode frequency from the TAE range down into the much lower frequency range of fishbones (discussed in section 4), and in fact strong coupling of fishbone and TAE modes can be observed. This large frequency range can make identification of the modes somewhat subjective. They typically appear as a sequence of bursts at progressively lower frequency, and the measured mode structure does not change significantly during this frequency evolution: it is clear that the bursts indicate the multiple excitation of a single mode. The initial mode frequency is in the TAE gap, while the final frequency is well below the gap, and can be close to zero in the core plasma rest frame. In the early years of MAST operation, bursting modes in the TAE frequency range were observed to chirp simultaneously to both higher and lower frequencies, as shown in figure 2 [28]. This type of frequency-sweeping behaviour, which has also been observed in conventional tokamaks, has been attributed to the formation of holes and clumps in the fast particle phase when the net growth rate of the mode is comparable to the collision frequency. The variation of frequency chirp $\delta\omega$ with time t for individual bursts in figure 2 is broadly consistent with a scaling $\delta\omega \propto t^{1/2}$ which had been predicted prior to the MAST measurements on the basis of a simplified model with only two phase space variables [29]. Since the constant of proportionality in this scaling depends on the linear growth rate of the mode (in the absence of damping) and the damping rate from

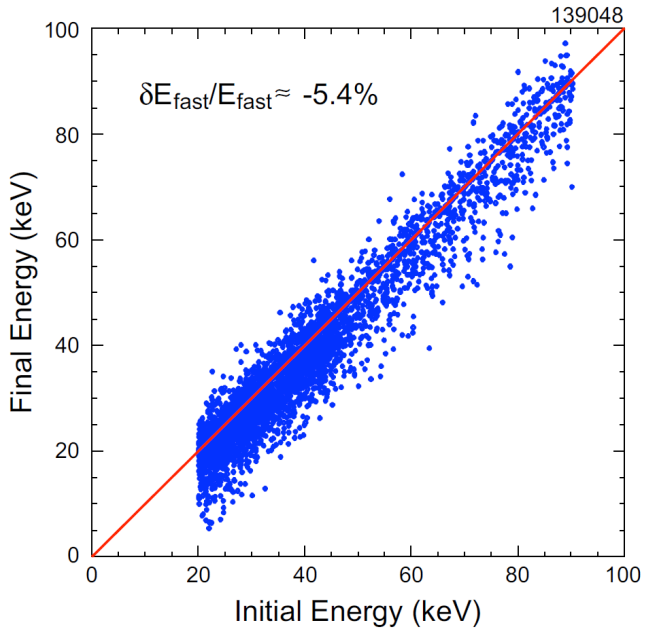

Figure 1: Final versus initial particle energies from an ORBIT simulation of the interaction of beam ions with multiple TAEs in NSTX discharge 139048. Measurements of mode amplitude, structure and frequency evolution were all used in the simulation. The red line corresponds to no energy loss or gain. (Reproduced from [23] with permission from IAEA.)

background dissipation, it is possible to infer information on these parameters from the experimentally-measured chirping rate. Several authors have explored this type of reduced model further, using various forms of the collision operator. Simulations in full ST toroidal geometry carried out using the guiding centre wave-particle HAGIS code, with collisional effects included, have also recovered qualitatively the phenomenon of simultaneous up and down frequency sweeping [30]. The importance of this work lies chiefly in the fact that fusion α-particle-driven TAEs in ITER are likely to be excited in a similar, weakly-unstable regime, with collisions playing a significant role in governing the nonlinear mode behaviour.

An alternative to the HAGIS approach is to construct reduced numerical models. In one such model, developed by Podestà and co-workers [31, 32], the energetic particle guiding centres are tracked using the NUBEAM module of the TRANSP plasma simulation code [33], with a sequence of "kicks" ΔE and ΔP_φ applied to each particle's energy E and toroidal canonical momentum P_φ. When the kicks are caused by interaction with a mode of frequency ω and toroidal mode number n, it follows immediately from Hamilton's equations that [31]

$$\Delta P_\varphi = \frac{n}{\omega}\Delta E. \tag{4}$$

The kicks are sampled from a probability distribution that is pre-calculated numerically by tracking particle orbits in equilibrium fields perturbed by one or more TAEs. Ap-

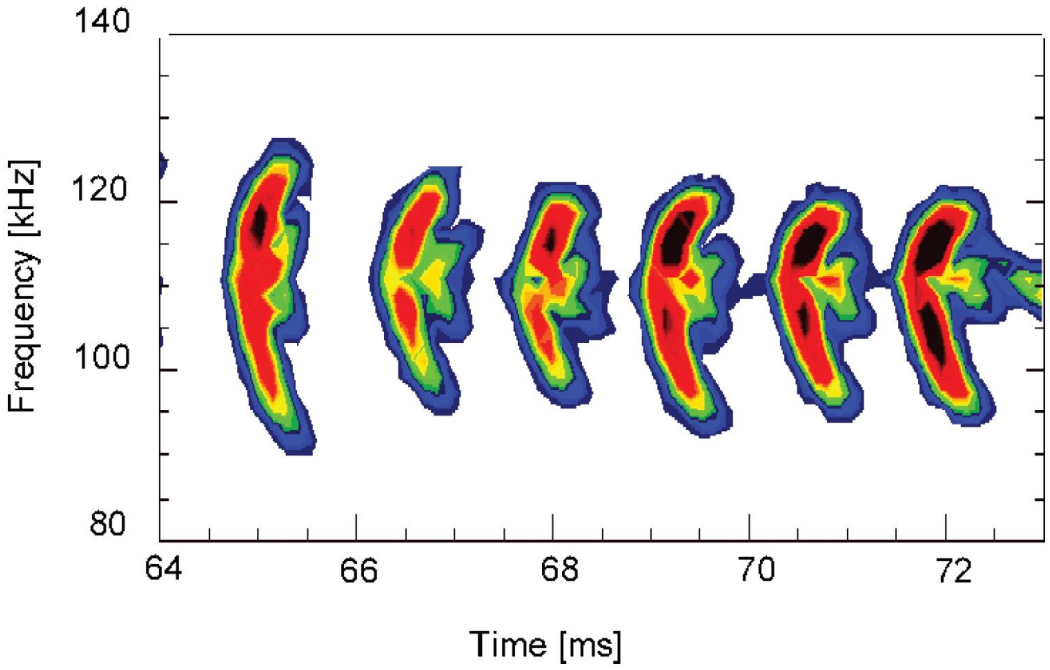

Figure 2: Magnetic spectrogram showing up and down frequency-sweeping $n = 1$ core-localized mode in TAE frequency range in MAST pulse 5568. (Reproduced from [28] with permission from IOP Publishing.)

plying this model to an NSTX pulse with strong TAE activity, Podestà and co-workers [32] found that both this approach and a simple *ad hoc* diffusion model reproduced fairly well the experimentally-measured temporal evolution of the total neutron flux (which was considerably lower than the flux predicted on the assumption of classical energetic particle confinement). However the distribution functions computed using the two models differed considerably, with significant pitch angle broadening occurring at low energy in the kick simulation but not in the *ad hoc* diffusion simulation. Such differences are potentially rather important, since pitch angle scattering is likely to have little or no effect on the total neutron flux but could have a significant impact on the neutral beam current drive. In principle it should be possible to validate the kick model by comparing its predictions with measurements obtained using diagnostics capabale of resolving details of the energetic particle distribution function, such as FIDA.

3.2 Alfvén cascades (reverse-shear Alfvén eigenmodes)

In addition to TAEs, tokamak plasmas with a region of reversed magnetic shear, and hence an off-axis minimum in q, can support energetic particle-driven shear Alfvén modes known as Alfvén cascades (ACs). These have been detected in several conventional aspect ratio tokamaks, and can be identified by a large upward sweep in frequency on timescales characteristic of the current profile evolution. The use of a

motional Stark effect (MSE) diagnostic on NSTX demonstrated clearly the presence of reverse shear during the current ramp-up phase, but no ACs were detected, despite the presence of beams which might have been expected to excite these modes. This was attributed by Fredrickson and co-workers [34] to coupling between ACs and geodesic acoustic modes arising from finite plasma pressure. When this coupling is taken into account, it is predicted that the AC frequency sweeps upward from the GAM frequency ω_{GAM} to the TAE gap frequency, ω_{TAE} [35]. In the limit of large aspect ratio and circular flux surfaces, the ratio of these two frequencies is given approximately by the expression [34]

$$\frac{\omega_{\mathrm{GAM}}^2}{\omega_{\mathrm{TAE}}^2} = 4q^2\beta_e\left(1+\frac{7}{4}\frac{T_i}{T_e}\right). \tag{5}$$

Here T_e, T_i are the electron and ion temperatures, and $\beta_e = 2\mu_0 n_e T_e/B^2$ is the electron plasma beta, where μ_0 is the permeability of free space, n_e is electron density and B is total magnetic field. The GAM frequency can be strongly modified by plasma shaping effects as well as finite aspect ratio, and so (5) should be treated with some caution when applied to NSTX or MAST. The key point is that the square of the frequency ratio increases with β_e, which tends to be higher in STs than inconventional tokamaks due to the use of low toroidal fields. Indeed this quantity is often sufficiently high that ω_{GAM} is comparable to or greater than ω_{TAE}, so that the predicted range of the frequency sweep given by (4) shrinks to zero and therefore ACs are not seen. However, in very low density, low β_e plasmas on NSTX, AC modes were observed, and their frequency evolution was used to estimate the evolution of the minimum safety factor, q_{min} [34] (see figure 3). Alfvén cascades were also detected in MAST pulses with moderate NBI power ($\leq 2\,\mathrm{MW}$), and, as in NSTX, were used to deduce information on the temporal evolution of the q-profile [36].

3.3 Compressional and global Alfvén eigenmodes

Alfvénic modes (identified as such by a linear scaling of mode frequency with magnetic field and an inverse scaling of frequency with the square root of density) are commonly seen in STs at frequencies well above those of TAEs, extending up to the ion cyclotron range. The first such modes to be detected in NSTX [13, 37, 38] were observed to propagate toroidally counter to the neutral beam injection direction, that is to say with parallel wave numbers $k_\parallel < 0$ (taking the mode frequency and the co-current toroidal direction to be both positive). The modes were clearly driven by energetic beam ions, which were injected in the co-current direction and thus had parallel velocity $v_\parallel > 0$. Neglecting perpendicular drift effects, modes excited in the ion cyclotron range through a wave-particle resonance satisfy the condition

$$\omega - \ell\Omega_i - k_\parallel v_\parallel = 0, \tag{6}$$

where Ω_i is the ion cyclotron frequency and ℓ is an integer. If $k_\parallel v_\parallel < 0$, as in the case of the modes reported in [13], it is apparent from (6) that these modes must have been excited through the normal Doppler resonance, $\ell > 0$, and it was generally found that the $\ell = 1$ resonance could account for the measured frequencies. These modes

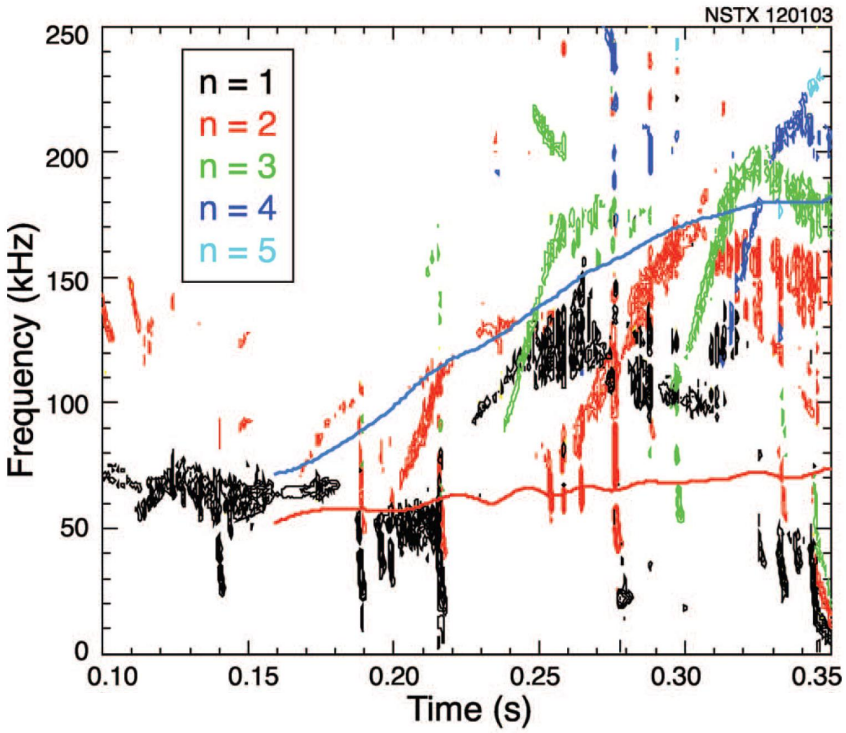

Figure 3: Spectrogram of Mirnov coil signal for low density discharge 120103 in NSTX, showing AC modes with $n = 2$ and 3 (identified by strong upward frequency sweeps). The red and blue curves indicate respectively the approximate GAM and TAE frequencies at the assumed mode location; $q_{\min}$ inferred from the AC modes was used to estimate the TAE frequency. (Reproduced from [34] with permission from American Institute of Physics.)

were at first all believed to be compressional Alfvén eigenmodes (CAEs), first studied theoretically in the specific context of ST geometry by Gorelenkova and Gorelenkov [39]. CAEs are related to ion cyclotron emission (ICE) detected in conventional tokamaks with energetic ion populations resulting from fusion reactions, ICRF heating or, in some cases, neutral beam injection. It was later realized that some of the high frequency modes detected in NSTX could be global Alfvén eigenmodes (GAEs), the shear-polarized complement to compressional Alfvén waves [40]. Being shear Alfvén waves, GAEs cannot exist above the ion cyclotron frequency, whereas CAEs can do so, and in general GAEs can be excited at lower frequencies than CAEs. A more subtle way of distinguishing between the two types of mode arises from differences in their dispersion relations [40]. The mode frequencies of GAEs lie just below the minimum values across the plasma of $k_{\|}c_A$ where $k_{\|} \simeq (n - m/q)/R$, m being poloidal mode number. When q is evolving in time, it is evident from this expression that the frequencies of GAEs with particular combinations of mode numbers can evolve in different ways, and can even cross over: this has been observed in NSTX [40]. Magnetic fluctuations in MAST at frequencies well above the TAE range were found to be elliptically polarized at the plasma edge with a significant magnetic field component parallel to the equilib-

rium field [41], suggesting that these modes could be identified as fast (compressional) Alfvén waves, i.e. CAEs. However, as explained below, polarization measurements at the plasma edge do not necessarily provide a definitive identification of modes in this frequency range.

In recent years co-propagating modes identified as CAEs have been detected at frequencies comparable to or below Ω_i in both NSTX [42] and MAST [43]. In such cases $k_\parallel v_\parallel > 0$, and it is apparent from (6) that any modes of this type detected at $\omega < \Omega_i$ must be excited via either the Landau resonance ($\ell = 0$) or the anomalous Doppler resonances, i.e. $\ell < 0$. The co-propagating modes in NSTX were attributed to the Landau resonance [42], whereas those reported in MAST could be explained by invoking the $\ell = -1$ anomalous Doppler resonance [43]. In the latter case the $\ell = -1$ resonance became relevant in pulses with relatively low toroidal field, in which ions at the full beam injection energy had speeds of up to $2.26 c_A$. In order to account for the resonant excitation of co-propagating CAEs with $\omega \ll \Omega_i$ it was necessary to take into account an additional grad-B and curvature drift term in (6) [43]. Modelling of the CAEs in one of these pulses, performed using `WHALES`, a cold plasma Hall-MHD code, yielded a large number of modes, with a frequency separation ($\simeq 40\,\mathrm{kHz}$) comparable to that of fine structure in the experimentally-measured spectrum. Figure 4 shows CAE eigenfunctions with frequencies in the ion cyclotron range computed for a MAST-like equilibrium using a similar code, `CAE3B` [44]. A notable feature of these modes is that they extend across the entire plasma cross-section, and as such differ from CAEs localised to the low field side magnetic "well" region of ST plasmas, studied by Gorelenkova, Gorelenkov and co-workers [39, 45]. If driven to sufficiently high amplitude, such global modes could affect the relaxation of energetic particle populations in the plasma core, not only at the plasma edge.

Since the experimentally-measured frequencies of CAEs and GAEs extend into the ion cyclotron range, it is necessary to include full orbit effects when modelling the energetic particle drive of these modes. One code that is suitable for this purpose is `HYM`, which models the evolution of fully kinetic fast ion populations and high frequency eigenmodes; the bulk electrons and ions are treated as a single fluid [46]. Simulations with this code have revealed the presence of both CAEs and GAEs [47], although these modes do not typically have "pure" compressional or shear properties, with the polarization changing as a function of radius. Thus, interpreting polarization measurements at the plasma edge is not straightforward.

Evidence has emerged that CAEs and GAEs can affect bulk plasma parameters in STs. Most strikingly, a correlation was found between the excitation of these modes and a degradation of electron heat confinement in NSTX [48]. One possible explanation for this degradation is that a resonant interaction occurred between the GAEs and trapped bulk electrons in the plasma core, with stochastic diffusion of the latter occurring due to the presence of multiple large amplitude GAEs with overlapping eigenfunctions [48]. An alternative possibility is that the presence of the high frequency modes modified the heat deposition profile of the neutral beams. `HYM` simulations of these plasmas indicate mode conversion of CAEs to kinetic Alfvén waves, and a consequent channelling of beam energy from the magnetic axis to the mode conversion region, at the edge of the beam density profile [49]. It has also been suggested that observations of CAEs

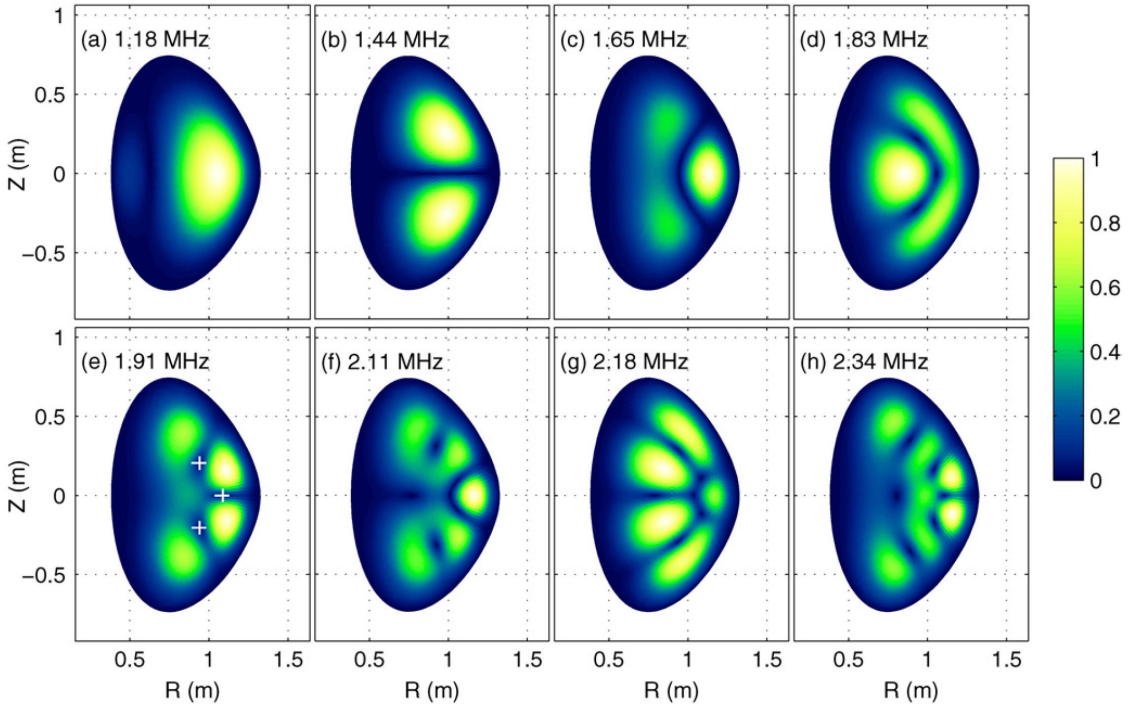

Figure 4: CAE eigenmodes with $n = 5$ computed for a MAST-like equilibrium using a cold plasma Hall-MHD code, `CAE3B`. The eigenmode frequencies are in the ion cyclotron range. (Reproduced from [44] with permission from IOP Publishing.)

in NSTX provide support for the concept of "alpha-channelling", that is to say the non-classical channelling of energetic particle energy directly into fuel ions rather than electrons [50].

CAEs and GAEs could in principle affect the temporal evolution of the energetic particle population that drives them, as in the case of TAEs. In some NSTX discharges with strong GAE activity, transient flux enhancements of up to a factor of ten have been observed in NPA spectra at energies close to the full neutral beam injection energy [51]. Fast particle-driven modes (other than GAEs) and low frequency MHD modes were absent or weak in these pulses, suggesting that a resonant interaction between the fast ions and the GAEs could provide an explanation for the flux enhancements. There are also indications that GAEs could have indirectly affected fast ions in NSTX by triggering TAE avalanches [52].

The properties of CAEs in the ion cyclotron range are predicted to be modified when there are two bulk ion species with unequal cyclotron frequencies, as in the deuterium-tritium plasma of a fusion reactor. The reason for this modification is that in such plasmas there are additional ion-ion hybrid resonances at frequencies between the cyclotron frequencies of the two ion species, and these resonances can act as sinks of wave energy: CAEs are predicted to be strongly-damped when the resonances are present [53]. This prediction was tested in MAST by gas puffing hydrogen into deuterium plasmas, producing pulses with different proportions of the two species. Figure 4 consists of spectrograms showing high frequency magnetic fluctuations in

three such pulses, with (a) no hydrogen gas puff, (b) 100 ms of hydrogen gas puff and (c) 180 ms of hydrogen gas puff [54]. The pulses were similar to each other except for the hydrogen-deuterium mix, which was monitored using measurements of neutron fluxes and edge Balmer-alpha emission (exploiting the small disparity between the wavelengths of Dα and Hα light due to the difference in nuclear mass). As the hydrogen content is increased, it is apparent that first the highest frequency CAEs disappear, and then essentially all of them disappear.

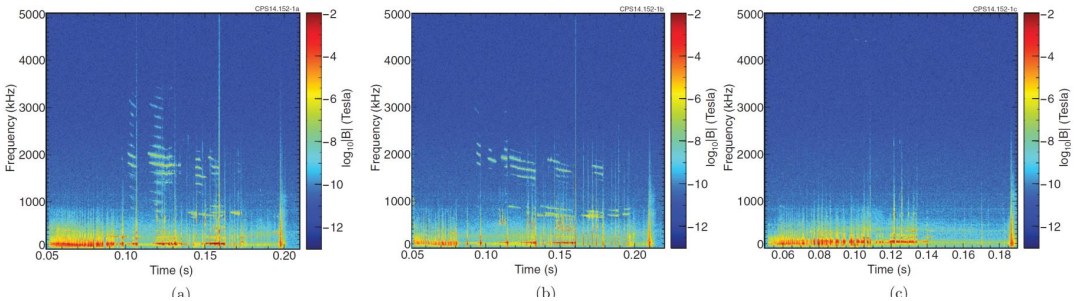

Figure 5: Spectrograms showing magnetic fluctuations in MAST pulses (a) 30457 (no H gas puff), (b) 30463 (100 ms gas puff) and (c) 30471 (180 ms gas puff). (Reproduced from [54] with permission from IOP Publishing.)

The observations of CAE suppression were interpreted by Oliver and co-workers [54] using a one-dimensional cold plasma model which was developed for highly-elongated STs [53], and is justifiable for these MAST plasmas, since the plasma elongation (defined as the ratio of plasma height to midplane width) during the period of CAE excitation was typically about 2.0. Modelling of the resonances and cutoffs in this model was found to be in agreement with the observations, lending support to the hypothesis that the CAEs were suppressed due to mode conversion at ion-ion hybrid resonances. This suggests that CAEs with frequencies in the ion cyclotron range in an ST deuterium-tritium burning plasma may also be suppressed.

While CAEs and GAEs can be excited in conventional tokamaks as well as STs, they are of particular interest in the ST context because they are likely to be the dominant energetic particle-driven modes in the high beta ($\beta \simeq 1$) plasma of an ST power plant: in these conditions any modes driven via the Landau resonance [corresponding to $\ell = 0$ in (6)], such as TAEs, will be strongly Landau damped [53]. If excited in an ST power plant, CAEs and GAEs could cause non-classical relaxation of the fusion α-particle distribution, and so it is important to study their properties in existing devices.

4 Fast particle-driven kink modes

4.1 Fishbones

In conventional aspect ratio tokamaks the fishbone instability is most commonly attributed to a resonance between an $m = n = 1$ internal kink mode and the toroidal

precession of trapped fast ions (although fishbones excited by passing fast ions have also been observed in conventional tokamaks). In STs, with high β and low toroidal field, the precession frequency can be quite low, or even negative (meaning that ions precess toroidally in the counter-current direction) in the presence of a magnetic well. Fishbone-like modes were frequently observed in NSTX, and it was conjectured that they were excited through a resonance with the bounce motion of fast ions [55]. In MAST fishbones (sometimes referred to as $n = 1$ energetic particle modes) and their effects on fast ion redistribution have been studied using several diagnostics, including the fission chamber and neutron camera [27, 56], FIDA [57, 58] and the soft X-ray camera [14].

Perhaps the clearest demonstration of the effects of these modes on fast particle confinement in ST plasmas was provided by Turnyanskiy and co-workers, who compared experimentally-measured radial profiles of neutron emission in MAST with synthetic profiles generated using `NUBEAM/TRANSP` [27]. By operating MAST plasmas in single-null configurations, with the magnetic axis below the geometric midplane of the vacuum vessel, it was possible to inject the neutral beams in such a way that the beam deposition profiles lay entirely outboard of the plasma magnetic axis. Off-axis NBI produced broader fast particle profiles than on-axis injection into double-null plasmas, thereby affecting the drive for instabilites driven by these particles. In general, any magnetic field perturbation with frequency ω and toroidal mode number n that conserves magnetic moment (approximately valid for modes in the fishbone frequency regime) has a growth rate that depends on a linear combination of two gradients in the fast ion distribution function f_b [59]:

$$\gamma \propto \omega \frac{\partial f_b}{\partial E} + n \frac{\partial f_b}{\partial P_\varphi}, \tag{7}$$

where, as before, E is particle energy and

$$P_\varphi = mRv_\varphi - Ze\psi, \tag{8}$$

is toroidal canonical momentum. In (7) m, Ze and v_φ are particle mass, charge and toroidal velocity while ψ is poloidal flux, defined such that the poloidal magnetic field is $\nabla\varphi \times \nabla\psi$. With this definition of ψ, a plasma current directed in the positive φ direction would correspond to ψ increasing from the magnetic axis to the plasma boundary. For fishbones in MAST, the $\partial f_b/\partial P_\varphi$ term in (6) is generally dominant, and it is apparent from (8) that the radial derivative of the fast ion distribution $\partial f_b/\partial\psi$ provides a measure of the growth rate, with $\partial f_b/\partial\psi < 0$ driving instability (i.e. $\gamma > 0$). Thus, by using off-axis rather than on-axis NBI in MAST it was possible to reduce the fishbone drive, and hence the level of fast particle redistribution.

When on-axis NBI was used in the MAST pulses discussed in [27], a doubling of the beam power produced only a modest increase (much less than a factor of two) in the neutron rate, as shown by the crosses in the left frame of figure 6. This was far short of the predicted neutron yield based on the assumption of purely classical confinement, which is indicated by the solid black curve in the figure. By assuming an anomalous fast particle diffusivity $D_{\rm an}$ of $2 - 3\,{\rm m^2 s^{-1}}$, it was possible to reproduce the measured neutron profile. In the case of off-axis NBI, on the other hand, a doubling of

the NBI power produced a similar increase in the neutron rate (see right frame of figure 6), and the level of anomalous fast ion diffusivity needed to reproduce the measured profile was $0.5\,\mathrm{m^2 s^{-1}}$ or less. It should be noted, however, that the maximum absolute neutron rate obtained with off-axis NBI was only slightly higher than that obtained with on-axis injection (the two parts of the figure have the same vertical scale).

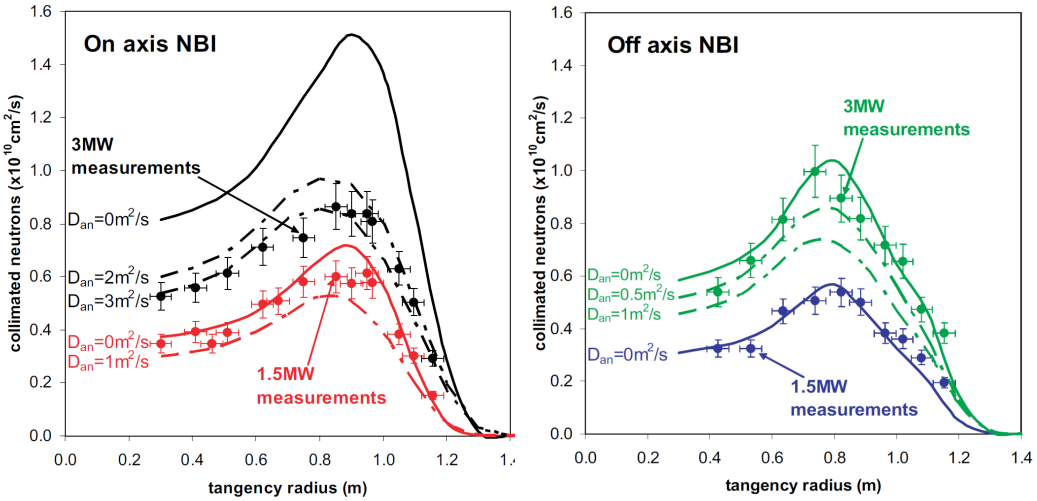

Figure 6: Measurements (crosses) and TRANSP simulations (curves) of neutron camera (NC) flux as a function of NC tangency radius in MAST plasmas with on-axis NBI (left) and off-axis NBI (right). The quantity D_{an} is the level of anomalous fast particle diffusivity used in the TRANSP simulations. (Reproduced from [27] with permission from IAEA.)

The conditions required in MAST to avoid significant fishbone-induced fast particle redistribution in double-null plasmas (with on-axis NBI) were studied more extensively by Keeling and co-workers [3]. It was found that by increasing the plasma density during the period of fishbone excitation by approximately a factor of two in a sequence of otherwise similar pulses, the mode amplitudes dropped to a negligible level. This is a simple consequence of the fact that under steady-state conditions the beam ion density and its radial gradient increase with the collisional slowing-down time, which scales inversely with the density. Again using `NUBEAM/TRANSP` to model the fast ion distribution, Keeling and co-workers demonstrated a correlation between the maximum value of $|\partial f_b/\partial\psi|$ in the vicinity of the mode, the mode amplitude, and the magnitude of fast ion redistribution [3].

It was noted in section 2 that FIDA spectra provide direct measurements of the fast ion velocity distribution; as such they can provide valuable information on which regions of fast ion phase space are most susceptible to fishbone-induced redistribution. Jones and co-workers [58] concluded from FIDA and neutron camera data that fishbones in MAST strongly affected passing beam ions at the highest energies, up to around 70 keV. This result can be usefully compared with figure 7, which is a plot of

the quantity $1/\Omega$ where

$$\Omega = |\omega - \langle\omega_\varphi\rangle - p\langle\omega_\theta\rangle|. \tag{9}$$

Here, ω is now the fishbone frequency (taken to be 30 kHz in figure 7), ω_φ, ω_θ denote toroidal and poloidal transit frequencies (for passing particles) or bounce frequencies (for trapped particles), angled brackets indicate orbit averages, and p is an arbitrary integer. Wave-particle resonances are represented by values of Ω close to zero, i.e. large values of $1/\Omega$, as plotted in figure 7. The parameter λ is particle pitch, $v_\parallel/v$. The toroidal and poloidal frequencies were computed using `HAGIS` for particles passing through a point in the outer midplane ($R \simeq 1.2$ m) where the fast ion pressure gradient was largest, and hence the fishbone instability drive was highest. The resonance condition is satisfied by both trapped and passing fast ions, in the latter case with energies ranging up to the full injection energy. This result, together with the experimental conclusion of Jones and co-workers noted above, suggests that the highest energy passing ions in MAST were redistributed via a resonant (rather than a non-resonant) interaction with the fishbones. It should be noted that resonance plots such as figure 7 indicate which fast ions are driving the mode, as well as which ones are most likely to be transported by it. The actual strength of the overall wave-particle interaction will of course depend on the local fast ion distribution, which is not taken into account in figure 7.

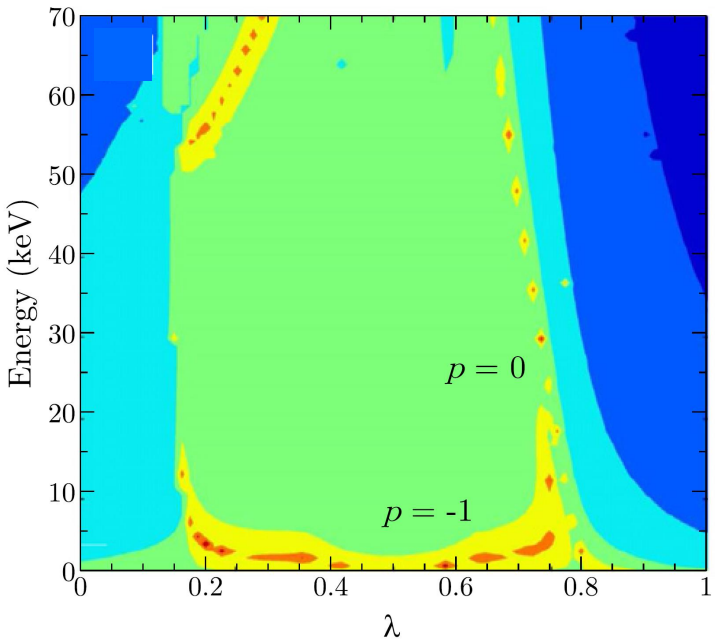

Figure 7: Resonance map in energy-pitch space at $R \simeq 1.2$ m in the outer midplane of MAST pulse 29976, showing the strength of interaction between fast ions and a fishbone with frequency 30 kHz and toroidal mode number $n = 1$. The plotted quantity is $1/\Omega$ where $\Omega = |\omega - \langle\omega_\varphi\rangle - p\langle\omega_\theta\rangle|$, with colours from blue to red indicating increasing values of $1/\Omega$. (Reproduced from [22] with permission from IOP Publishing.)

As discussed above, modelling of fast ion redistribution due to fishbones has been

performed in an *ad hoc* manner through the use of empirical anomalous diffusion coefficients in NUBEAM/TRANSP, but no completely self-consistent computations of this process have been carried out. HAGIS has been used to model the effects of fishbones on beam ions in MAST, with the eigenmode structure calculated using the MISHKA code and the mode amplitude evolution matched to experiment [60]. This modelling indicates that the levels of anomalous fast ion diffusivity found by Turnyanskiy and co-workers [27], i.e. $D_{\rm an} = 0.5\,{\rm m}^2{\rm s}^{-1} - 3\,{\rm m}^2{\rm s}^{-1}$ can be explained by fishbones with amplitudes in the range $\delta B/B = 10^{-3} - 5 \times 10^{-3}$. These figures are credible, although it is not straightforward to verify them by measuring the fishbone amplitude *in situ*, since magnetic coil measurements provide only the amplitude outside the plasma. An alternative possible approach to modelling the effects of fishbones on fast particles in STs would be to retain the NUBEAM/TRANSP framework and adapt the kick model used to describe the effects of TAEs in NSTX [31, 32]. The need for physics-based modelling is underlined by the fact that purely diffusive *ad hoc* models of fishbone-induced fast particle transport fail to reproduce some of the neutron profiles and FIDA spectra which have been measured in MAST [56, 58].

4.2 Saturated kink modes

Fishbones in MAST often evolved into steady, non-chirping modes at similar frequency (close to the core plasma toroidal rotation frequency): these were identified as saturated $n = 1$ internal kink modes in plasmas with $q > 1$ in the core region [61]. Measurements carried out with a wide range of diagnostics showed that these long-lived modes (LLMs) caused significant energetic particle redistribution [22]. Figure 8 shows a slight drop in total neutron emission after the start of LLM excitation, indicated by a dashed line. Typically, as in this case, the neutron rate recovered after a drop in the mode amplitude. Saturated internal kink modes were also often observed in high β NSTX plasmas and, as in MAST, they caused a measurable drop in the total neutron rate which then recovered after the mode amplitude fell [62]. The USXR diagnostic on NSTX could be used to measure directly the $m = n = 1$ structure of these modes.

A MAST plasma with a saturated internal kink mode can be thought of as consisting of a helical core embedded inside an axisymmetric outer region. This prompted Pfefferlé and co-workers [63] to use a three-dimensional code, ANIMEC, for the purpose of modelling the equilibrium fields in such a plasma, and a guiding-centre code, VENUS-LEVIS, to compute the effects of the helical core on energetic ion confinement. Simulations carried out for a range of LLM amplitudes were used to generate synthetic neutron camera profiles, which were found to be in broad agreement with measured profiles. The drops in neutron emission were found to be caused mainly by redistribution of fast ions rather than losses, with a consequent outward shift in the fast ion current drive profile.

In an earlier experimental study Menard and co-workers reached similar conclusions with regard to the effects of LLMs in NSTX [64], based on direct measurements of the current profile (using a motional Stark effect diagnostic) and NUBEAM/TRANSP simulations of the neutron rate. Although LLMs appear to have caused relatively few fast ion losses in MAST or NSTX plasmas, it is clear that they produced large enhancements

in the transport of these particles within the plasma: depending on the assumed radial extent of the mode, it was found that anomalous diffusivities in the plasma core of between $20\,\mathrm{m^2 s^{-1}}$ and $50\,\mathrm{m^2 s^{-1}}$ were needed to reproduce the measured neutron rates during LLM excitation in NSTX [64].

5 Redistribution of fast ions due to non-resonant instabilities

The confinement of energetic particles in STs can in principle be affected by any instability, not only those driven by the energetic particles themselves. Energetic particle losses in NSTX H-mode plasmas, for example, were observed to be correlated with various MHD modes [65]. In this section we consider briefly the effects on fast ions of two key instabilities that affect the core and edge regions of ST plasmas.

5.1 Sawteeth

Experimental studies of the effects of sawtooth on fast particle redistribution in MAST are briefly described in [22]. As in conventional tokamaks, the confinement of energetic ions in the core regions of STs can be strongly affected by sawtooth crashes. An extreme example of this can be seen in figure 9, which consists of time traces in a sawtoothing MAST discharge obtained using the fusion proton detector (top), the neutron camera (middle) and the fission chamber (bottom) [6]. Large drops can be seen in every signal at each crash, particularly the first one at about 0.225 s, but in one particular neutron camera channel the flux was reduced by well over a factor of two (see red curve in middle plot). Despite these extreme changes in the fusion yield in some parts of the plasma, FIDA measurements during MAST sawtooth crashes suggest a relatively modest drop in overall fast ion confinement inside the sawtooth inversion radius, although it is interesting to note that, as in the case of fishbones, passing beams ions at the highest energies are among those that are affected [22]. Since, as noted in section 2, the fusion cross-section is a strongly-increasing function of energy, the loss (or redistribution to regions of lower bulk ion density) of a relatively small number of beam ions close to the full injection energy could have a large impact on the fusion yield, thereby accounting for drops as large as those shown in figure 9.

Simulations of the effects of sawtooth crashes on fast particles have been carried out for one particular MAST pulse (29880), using Kadomtsev's model for the reconnecting fields in `NUBEAM/TRANSP` [33] with D_{an} set equal to zero at all times. Synthetic neutron camera profiles before and after a sawtooth crash, computed using these simulations, were found to be in remarkably good agreement with measured profiles [22]. The `NUBEAM` simulations indicated a reduction in the passing fast ion population inside the sawtooth inversion radius, and an increase in the trapped population (due to pitch angle scattering of passing ions). This last result is not entirely consistent with FIDA measurements carried out using a vertical viewing system, which indicate that trapped energetic ions were redistributed by sawtooth crashes along with passing ones [22]: this discrepancy may reflect limits in the applicability of the MHD-based Kadomtsev model

to sawteeth in MAST.

Sawtooth crashes in NSTX have been observed to cause drops in neutron emission that are comparable to those shown in figure 9 [66]. Simulations of the effects of such crashes on energetic particle confinement have been carried out, again using a Kadomtsev-type model for the reconnecting fields, but this time with the particles being tracked with a full orbit code, `GYROXY` [66]. Full orbit effects are likely to play an important role, given the evidence from MAST that the highest energy fast ions seem to be most susceptible to sawtooth-induced redistribution or loss, and indeed the `GYROXY` simulations suggest that cyclotron resonances (not represented in the guiding centre `NUBEAM` simulations reported in [22]) enhanced the level of stochasticity in fast ion orbits, thereby increasing the extent to which the ions were redistributed.

5.2 Edge localised modes

Until recently little attention had been given to the possibility that edge localised modes (ELMs) could have a significant effect on the confinement of fast particles in either conventional or spherical tokamaks, probably because of the fact that fast ion distributions are often strongly-peaked in the plasma centre whereas ELMs, as the name suggests, affect mainly the pedestal region at the edge of H-mode plasmas. However ELM-induced fast ion losses have been reported in several medium-sized conventional tokamaks [67], and, as discussed earlier, relatively broad fast ion distributions were produced in single null MAST plasmas with off-axis NBI. While the use of such configurations helps to suppress fast ion-driven instabilities and consequent fast ion redistribution [27], it also means that fast ions are more likely to be affected by edge perturbations such as ELMs.

Klimek and co-workers have recently carried out a statistical study of the effects of ELMs on neutron emission in MAST plasmas with and without resonant magnetic perturbations (RMPs) which were applied for the purpose of mitigating the ELMs [68]. The direct effects of RMPs themselves on energetic particle confinement will be discussed in the next section. Figure 10 shows distributions of relative changes in neutron emission ΔR following RMP-mitigated ELMs and unmitigated ELMs in single null plasmas with two different plasma currents; $\Delta R > 0$ indicates a *reduction* in neutron flux. All of the distributions peak at values of ΔR that are comparable to or less than the distribution width, and therefore any non-null result inferred from these plots is of marginal statistical significance at most. Nevertheless figure 10 indicates that unmitigated ELMs are weakly correlated with a reduction in neutron emission, and hence in fast ion confinement, at least in 600 kA plasmas. In this case the mean value of ΔR is about 0.06, and the standard deviation of the distribution is comparable to this. On the other hand, there is no clear evidence here of RMP-mitigated ELMs having a net effect on neutron rates: the peaks of these distributions are very close to $\Delta R = 0$. These results suggest that, in addition to mitigating or suppressing ELMs, resonant magnetic perturbations could in some circumstances have a beneficial impact on energetic particle confinement (notwithstanding the *de*confining effect of three-dimensional static fields, discussed below). However it may be expected that more clear-cut evidence for ELM-induced energetic particle losses will emerge from MAST-Upgrade, since, as discussed in section 2, this device will be equipped with a

fast ion loss detector.

6 Redistribution of fast ions due to static field perturbations

The exact toroidal symmetry of tokamak plasmas is broken by both MHD instabilities with $n \neq 0$ and by static magnetic field perturbations arising from currents outside the plasma. Any such perturbations could in principle lead to a degradation in the confinement of fast particles, since their toroidal canonical momentum P_φ is no longer a constant of the motion in the collisionless limit. The energies and pitch angles of beam ions in MAST are such that the toroidal angular momentum term in (8) can be comparable to the poloidal flux term, and so trapped beam ions, which undergo a reversal in v_φ at the bounce points, can have radial excursions comparable to the plasma minor radius, as shown in the right hand frame of figure 11. Beam ions with orbits of this type are particularly vulnerable to being lost from the plasma due to static three-dimensional field perturbations, since the latter tend to be strongly localised to the low field side plasma edge.

The use of a finite number of toroidal field coils invariably produces a ripple in the equilibrium field, the effects of which on fast ion confinement in MAST have been modelled and found to be small: the reduction in beam heating power due to ripple losses was estimated to be less than 1% [69]. Similar calculations for a proposed ST power plant and a proposed ST components test facility also show that fewer than 1% of fusion α-particle would be lost from these devices due to ripple transport in the collisionless limit [70]. The low level of ripple losses is due in part to the presence of a relatively large poloidal field close to the outer plasma boundary (an inherent feature of tight aspect ratio tokamaks), which constricts the orbits of trapped energetic ions and prevents them from traversing regions with a high ripple amplitude.

Three-dimensional field perturbations arising from RMPs have been used to mitigate ELMs in MAST and NSTX. In general these are likely to have a greater impact than toroidal field ripple on fast particle confinement, since the perturbation amplitudes inside the plasma tend to be higher. Figure 12 shows time traces from two single-null MAST pulses with (black curves) and without (red curves) RMPs with dominant toroidal mode number $n = 3$ [71]. There is a clear drop of nearly a factor of two in the neutron rate (figure 12b) shortly after the application of RMPs in pulse 30086 which is absent in the pulse without RMPs (30090). Similar drops in the fusion proton rate and FIDA emission were also recorded during RMPs in pulse 30086, while drops in neutron camera fluxes were recorded in other pulses with RMPs. As shown in figure 12c, ELMs occurring during the period of application of RMPs in pulse 30086 and during the corresponding period in pulse 30090 have similar amplitude and frequency, and hence it may be expected that they had a similar effect on fast ion confinement. Figure 12d indicates a somewhat lower level of MHD activity in pulse 30086 than in pulse 30090, which would be expected to result in a reduced level of MHD-induced fast ion redistribution in the former pulse. All of this suggests that the drop in neutron emission in pulse 30086 can be attributed to the RMP-induced violation of P_φ conservation,

and this is borne out by TRANSP modelling of this pulse using an axisymmetric equilibrium, which overestimates the neutron rate by about a factor of two during the period of application of the RMPs [71].

First principles-based modelling of fast particle transport and neutron emission in MAST pulse 30086 before and during the application of the RMPs has also been carried out using a non-steady-state version of the `OFMC` particle tracking code [72]. The RMPs were modelled using the vacuum approximation, toroidal field ripple was also taken into account, and beam ions were tracked using both full orbit and guiding centre schemes. Full orbit tracking was found to be essential in order to obtain approximate agreement between the measured and simulated neutron rates, due to the relatively large Larmor radii of beam ions in MAST. The most significant conclusion of this study was that the combination of RMPs and toroidal ripple caused the beam power loss fraction to rise from 30% in the axisymmetric limit to around 45%. The plasma current in this pulse was relatively low for MAST (400 kA), and for this reason fast ion confinement was relatively poor even in the axisymmetric limit, but the large additional degradation in beam heating found by Tani and co-workers is nevertheless a striking illustration of the fact that ELM mitigation through the use of RMPs may have adverse consequences for plasma performance. More modest levels of RMP-induced fast ion losses were observed in guiding-centre (`VENUS-LEVIS`) simulations of MAST reported by Pfefferlé and co-workers [73]. This may have been due in part to the fact that these authors used an up-down symmetric, double-null equilibrium: as discussed in section 4, fast ion distributions were more centrally-peaked (and therefore less susceptible to losses arising from edge perturbations) in double-null MAST plasmas than in single-null plasmas. Moreover, as noted above, Tani and co-workers [72] observed significantly more RMP-induced fast ion losses in full orbit simulations than in guiding centre ones, suggesting that the former approach may be required for accurate quantitative modelling of this process in MAST.

In NSTX it was found that RMPs significantly modified the behaviour of GAEs [74], in a manner not dissimilar to the effects of such perturbations on ELMs in MAST: as shown in figure 13, the degree of frequency chirping, the repetition period, and the amplitude of GAEs all dropped by a factor of 2-3 within 1 ms or so of the RMPs being applied. Modelling of the beam ion distribution in these pulses was carried out using the `SPIRAL` code, in the presence of the RMPs (with and without the plasma response taken into account) and in the axisymmetric limit. The beam ion distribution function f_b was calculated along curves in phase space corresponding to the normal Doppler cyclotron resonance condition for GAEs, corresponding to $\ell = 1$ in (6). It was found that losses due to the RMPs reduced $\partial f_b / \partial v_\perp$ (a measure of the GAE drive, $v_\perp$ being beam ion velocity perpendicular to the field) by a modest amount, around (10-20) % [74]. The Mirnov coil data shown in figure 13 suggest, in the light of this modelling result, that the mode properties are rather sensitive to the instability drive, which is to be expected in dynamical systems that are close to marginal stability. Thus, it may be possible to use RMPs to mitigate the effects of fast particle-driven Alfvénic instabilities as well as those of ELMs, and this could play an important role in optimising plasma performance, given the apparently adverse effects of the former on electron confinement in some NSTX plasmas [48].

7 Ion and electron acceleration

Although parallel electric fields are invariably present in tokamak plasmas, particle acceleration is normally suppressed by frictional drag forces. However reconnection events can produce changes in the parallel electric field that are large enough to accelerate both ions and electrons to highly supra-thermal energies. In this section we discuss two examples of scenarios in which particle acceleration is observed in ST plasmas.

7.1 Fast ion production due to magnetic reconnection

STs generally, including MAST, are susceptible to internal reconnection events (IREs), characterised by a broadening of the current profile, a small temporary rise in the total plasma current, and a spike in the loop voltage. The acceleration of both deuterons and protons was detected using the MAST NPA during Ohmic discharges, in which no energetic ions had been introduced to the plasma through external agents such as NBI or radio-frequency heating [75]. The absence of auxiliary heating in these discharges also meant that the fusion reaction rate was extremely low. The fast ion spectra observed in MAST could be accounted for by invoking an effective electric field determined by plasma impurities and particle trapping [75].

More recently, it has been demonstrated that ion acceleration also occurred during merging-compression startup of MAST plasmas [76]. In this startup process, plasma rings with parallel (and hence mutually-attractive) toroidal currents are formed around coils at the top and bottom of the vacuum vessel. The rings detach from the coils and merge in the vessel midplane, resulting in a single set of closed flux surfaces. As shown in figure 14, the magnetic reconnection associated with this merging process resulted in the acceleration of both deuterons and protons. Specifically this figure shows energy distribution functions for deuterium (squares/red curves) and hydrogen (circles/blue curves) obtained using the MAST NPA during the merging-compression phases of pulses 9081 (left) and 9180 (right), in both cases well before the start of NBI. The temporal evolution of the plasma current up to and beyond the merging phase was very similar in these two pulses, but in pulse 9081 the magnetic field used in the NPA was lower than its maximum value. This limited the diagnostic to the detection of thermal ions and relatively low energy suprathermal ions, thereby enhancing the energy resolution of the recorded spectrum (since the total number of channels was fixed). For each pulse the NPA fluxes were integrated in time over a period of 8 ms, covering the merging process.

The magnitude and duration of parallel electric fields found in two-fluid simulations of the merging process [77] are broadly consistent with the accelerated particle energies indicated by the NPA measurements. As in the case of IREs, the reconnection process during merging startup produced a small rise in the plasma current ΔI_p; the associated electromotive force implies an energy gain $\Delta E \propto \Delta I_p^2$, which is also consistent with the tail energies shown in figure 14 [76]. By identifying the low energy part of the deuterium distribution in the left hand frame of figure 14 with the bulk ion population, the accelerated ion fraction can be estimated to be of the order of 10^{-2}, but this is highly uncertain for a number of reasons, including the fact that the pitch angle distributions

of the deuterons and protons accelerated in these discharges are unknown. Quantitative modelling of particle acceleration during merging-compression startup in MAST has yet to be carried out, but numerical tools that could be used to simulate the acceleration of test particles in merging fields are readily available (e.g. [78]), and could be used for this purpose. Such modelling may help to shed light on particle acceleration in solar flare plasmas, since these have dimensionless parameters similar to those of MAST [76].

7.2 Fast electron production due to edge localised modes

In addition to being linked to fast ion losses, ELMs in MAST also caused electrons to be accelerated to energies in the tens of keV range [79]. Evidence for this first emerged in observations carried out using the Synthetic Aperture Microwave Imaging (SAMI) radiometer of microwave bursts a few tens of microseconds before peaks in Dα emission; the microwave intensities corresponded to brightness temperatures exceeding pre-ELM levels by up to four orders of magnitude, clearly indicating a nonthermal origin. Later, enhancements in soft X-ray emission from the plasma edge were found to coincide with the microwave bursts. Figure 15 shows the evolution of soft X-ray intensity (red curve) and Dα intensity (black curve) during a typical ELM in MAST. The X-rays had energies in the range 1-30 keV, and the X-ray time trace shown in figure 15 corresponds to a line-of-sight passing through the low field side plasma edge above the midplane.

It is well-established that the Dα spikes associated with ELMs are linked to the eruption of field-aligned filaments from the plasma edge. Simulations using the `JOREK` resistive MHD code have revealed the generation of parallel electric fields as high as $2\,\mathrm{kVm}^{-1}$ at the start of the filament eruption process [80]. These fields are sufficiently large and long-lasting to account for the acceleration of electrons to energies in the tens of keV range, which is suggested by the soft X-ray bursts. Like the co-propagating CAEs in MAST [43], the microwave bursts can be attributed to waves excited by the anomalous Doppler instability, in this case driven by strongly field-aligned energetic electron distributions via the resonance condition

$$\omega - \ell\Omega_e - k_\parallel v_\parallel = 0, \tag{10}$$

where Ω_e is the electron cyclotron frequency, $\ell = -1$ and $v_\parallel$ is now the parallel velocity of energetic electrons rather than ions. Simulations carried out using the `EPOCH` particle-in-cell code show that modes driven via this resonance condition have a range of frequencies in the Ω_e range, but only a simulation with relatively low electron density ($2 \times 10^{18}\,\mathrm{m}^{-3}$) produced strong instability at frequencies close to those of the experimentally-measured microwave bursts. This result provides further strong evidence that the site of energetic electron production is very close to the plasma edge. The role of these energetic electrons in ELM filament dynamics is not yet known, but could be considerable.

8 Prospects for energetic particle studies in NSTX-Upgrade and MAST-Upgrade

In recent years both MAST and NSTX have undergone major upgrades which are expected to expand the scope of energetic particle physics studies. The first physics campaign on NSTX-Upgrade has now taken place. Neutral beam heating experiments in this campaign have produced many of the energetic particle-driven instabilities that were previously observed in NSTX. However NSTX-Upgrade has three additional neutral beam sources, with tangency radii $R_{\rm tan}$ (defined as the major radii where the beamlines are tangential to flux surfaces) generally outside the magnetic axis, whereas in NSTX the neutral beams had tangency radii smaller than the magnetic axis radius. It has already been demonstrated that the added flexibility to control the fast ion distribution afforded by the three new neutral beam sources on NSTX-Upgrade offers an unprecedented ability to control instabilities excited by the super-Alfvénic fast ion population. For the first time, a TAE propagating counter to the plasma current has been excited, as predicted, by using neutral beam injection far from the magnetic axis to create a hollow fast ion profile. More importantly, it has been demonstrated that the same off-axis neutral beam source can be used to reliably and strongly suppress GAEs. It was observed that if beam sources were injected with $R_{\rm tan} = 1.1\,{\rm m}$ or $1.3\,{\rm m}$ outside the magnetic axis, which typically lies at $R_{\rm axis} \simeq 100\,{\rm cm}$, the high frequency Alfvénic activity was suppressed, or the level of the activity was reduced [81]. This was clearly seen in many shots where one of the new sources was turned on late or had a fault during GAE activity. The suppression occurs very soon after the source is turned on (typically within a few milliseconds), demonstrating that it is the perturbation to the fast ion distribution that is responsible for suppression, rather than equilibrium changes.

MAST-Upgrade will also have additional beams. When it first starts operating, it will have two beam sources, one on-axis ($R_{\rm tan} = 0.7\,{\rm m},\ = 0.0\,{\rm m}$), the other off-axis ($R_{\rm tan} = 0.8\,{\rm m},\ = 0.65\,{\rm m}$), each providing up to 2.5 MW. This will make it possible to produce a wide range of heating, current drive and fast ion profiles. Figure 16 shows computations performed with the `LOCUST` code of fast ion density profiles that are expected to be obtained in MAST Upgrade using on-axis NBI only (left plot), off-axis NBI only (middle plot), and with both beam sources (right plot) [82]. The use of relatively broad fast ion profiles is expected to reduce the drive for instabilities driven by these particles, and one of the research priorities will be to determine whether the current driven by off-axis NBI conforms to expectations based on classical confinement, or is degraded by fast particle-driven instabilities. In future campaigns it is hoped that additional beam sources will be added, eventually providing up to 12.5 MW; Keeling and co-workers [3] have shown that one of the additional beam sources can be configured in such a way that the drive for fishbones can be minimised, thereby optimising the beam heating and current drive that can be achieved. MAST-Upgrade (like MAST) will be equipped with RMP coils, and it is intended that the effects of RMP field perturbations on fast ion confinement will be studied systematically for a wide range of coil configurations and fast ion deposition profiles. As discussed earlier, although

broad fast ion profiles are less likely to drive instabilities, they are more susceptible to losses due to field perturbations at the plasma edge, and so the latter should be considered when evaluating the overall efficacy of different beam heating schemes.

9 Concluding remarks

It should be evident from the review presented in this paper that MAST and NSTX have provided a wealth of information on the behaviour of suprathermal ions and electrons in tight aspect ratio magnetically-confined plasmas, and a challenge to theoretical models. This information is obviously important for the development of the ST as a fusion reactor concept, but it also provides valuable insights into the likely behaviour of energetic particles in future conventional tokamak burning plasma devices such as ITER. For example, the availability in STs of super-Alfvénic neutral beams has made it possible to study in more detail than in conventional tokamaks the nonlinear evolution of Alfvén eigenmodes in the near-threshold conditions likely to prevail in ITER. The experimental studies and modelling of energetic particle redistribution due to Alfvén eigenmodes and fishbones in MAST and NSTX show that while *ad hoc* anomalous transport models have an important role to play in the interpretation of these experiments, it is absolutely necessary to develop more physics-based models (either reduced or fully-self consistent) of the redistribution process in order to develop a truly predictive capability for the behaviour of energetic ions in future devices, in particular predictions of the plasma heating and current drive provided by these particles.

Acknowledgments

This work has received funding from the RCUK Energy Programme [grant number EP/I501045]. To obtain further information on the data and models underlying this paper please contact PublicationsManager@ccfe.ac.uk.

References

[1] Menard J E *et al* 2016 *Nucl. Fusion* **56** 106023

[2] Bosch H-S and Hale G M 1992 *Nucl. Fusion* **32** 611

[3] Keeling D L *et al* 2015 *Nucl. Fusion* **55** 013021

[4] Cecconello M *et al* 2012 *Nucl. Fusion* **52** 094015

[5] Stammers K and Loughlin M J 2006 *Nucl. Instrum. Methods Phys. Res.* **A 562** 521

[6] Perez R V *et al* 2014 *Rev. Sci. Instrum.* **85** 11D701

[7] Medley S S and Roquemore A L 1998 *Rev. Sci. Instrum.* **69** 2651

[8] Tournianski M R, Carolan P G and Akers R J 2004 *Rev. Sci. Instrum.* **75** 2854

[9] Podestà M, Heidbrink W W, Bell R E and Feder R 2008 *Rev. Sci. Instrum.* **79** 10E521

[10] Michael C A *et al* 2013 *Plasma Phys. Control. Fusion* **55** 095007

[11] Darrow D S 2008 *Rev. Sci. Instrum.* **79** 023502

[12] Hole M J and Appel L C 2003 *Proc. 30th EPS Conf. on Controlled Fusion and Plasma Physics (St Petersburg, Russia, July 2003)* vol 27A P3.132

[13] Fredrickson E D *et al* 2001 *Phys. Rev. Lett.* **87** 145001

[14] Cecconello M *et al* 2015 *Nucl. Fusion* **55** 032002

[15] Stutman D, Finkenthal M, Soukhanovskii V, May M J, Moos H W and Kaita R 1999 *Rev. Sci. Instrum.* **70** 572

[16] Crocker N A *et al* 2011 *Plasma Phys. Control. Fusion* **53** 105001

[17] Hillesheim J C *et al* 2015 *Nucl. Fusion* **55** 073024

[18] Heidbrink W W, McKee G R, Smith D R and Bortolon A 2011 *Plasma Phys. Control. Fusion* **53** 085007

[19] Fu G Y and Van Dam J W 1989 *Phys. Fluids* B **1** 1949

[20] McClements K G *et al* 1999 *Plasma Phys. Control. Fusion* **41** 661

[21] Breizman B N and Sharapov S E 1995 *Plasma Phys. Control. Fusion* **37** 1057

[22] Cecconello M *et al* 2015 *Plasma Phys. Control. Fusion* **57** 014006

[23] Fredrickson E D *et al* 2013 *Nucl. Fusion* **53** 013006

[24] Podestà M *et al* 2010 *Phys. Plasmas* **17** 122501

[25] Hole M J, von Nessi G, Fitzgerald M and the MAST team 2013 *Plasma Phys. Control. Fusion* **55** 014007

[26] Podestà M *et al* 2009 *Phys. Plasmas* **16** 056104

[27] Turnyanskiy M *et al* 2013 *Nucl. Fusion* **53** 053016

[28] Pinches S D, Berk H L, Gryaznevich M P, Sharapov S E and JET-EFDA Contributors 2004 *Plasma Phys. Control. Fusion* **46** S47

[29] Berk H L, Breizman B N and Petviashvili N V 1997 *Phys. Lett. A* **234** 213

[30] Pinches S D *et al* 2012 *Proc. 24th IAEA Fusion Energy Conf. (San Diego, USA, 2012)* TH/P3-34

[31] Podestà M, Gorelenkova M and White R B 2014 *Plasma Phys. Control. Fusion* **56** 055003

[32] Podestà M, Gorelenkova M, Fredrickson E, Gorelenkov N N and R. B. White 2016 *Phys. Plasmas* **23** 056106

[33] Pankin A, McCune D, Andre R, Bateman G and Kritz A 2004 *Computer Phys. Commun.* **159** 157

[34] Fredrickson E D *et al* 2007 *Phys. Plasmas* **14** 102510.

[35] Breizman B N, Pekker M S, Sharapov S E and JET EFDA contributors 2005 *Phys. Plasmas* **12** 112506

[36] Gryaznevich M P *et al* 2008 *Nucl. Fusion* **48** 084003

[37] Gorelenkov N N *et al* 2002 *Nucl. Fusion* **42** 977

[38] Fredrickson E D, Gorelenkov N N and Menard J 2004 *Phys. Plasmas* **11** 3653

[39] Gorelenkova M V and Gorelenkov N N 1998 *Phys. Plasmas* **5** 4104

[40] Gorelenkov N N *et al* 2003 *Nucl. Fusion* **43** 228

[41] Appel L C *et al* 2008 *Plasma Phys. Control. Fusion* **50** 115011

[42] Fredrickson E D *et al* 2013 *Phys. Plasmas* **20** 042112

[43] Sharapov S E *et al* 2014 *Phys. Plasmas* **21** 082501

[44] Smith H M and Verwichte E 2009 *Plasma Phys. Control. Fusion* **51** 075001

[45] Gorelenkov N N, Cheng C Z and Fredrickson E D 2002 *Phys. Plasmas* **9** 3483

[46] Belova E V, Jardin S C, Ji H, Yamada M and Kulsrud R 2000 *Phys. Plasmas* **7** 4996

[47] Gorelenkov N N *et al* 2004 *Phys. Plasmas* **11** 2586

[48] Stutman D *et al* 2009 *Phys. Rev. Lett.* **102** 115002

[49] Belova E V, Gorelenkov N N, Fredrickson E D, Tritz K and Crocker N A 2015 *Phys. Rev. Lett.* **115** 015001

[50] Gorelenkov N N, Fisch N J and Fredrickson E D 2010 *Plasma Phys. Control. Fusion* **52** 055014

[51] Medley S S *et al* 2012 *Nucl. Fusion* **52** 013014

[52] Fredrickson E D *et al* 2012 *Nucl. Fusion* **52** 043001

[53] Lilley M K and Sharapov S E 2007 *Phys. Plasmas* **14** 082501

[54] Oliver H J C, Sharapov S E, Akers R, Klimek I, Cecconello M and the MAST Team 2014 *Plasma Phys. Control. Fusion* **56** 125017

[55] Fredrickson E D, Chen L and White R B 2003 *Nucl. Fusion* **43** 1258

[56] Klimek I *et al Nucl. Fusion* **55** 023003

[57] Jones O M *et al* 2013 *Plasma Phys. Control. Fusion* **55** 085009

[58] Jones O M *et al* 2015 *Plasma Phys. Control. Fusion* **57** 125009

[59] Heidbrink W W 2008 *Phys. Plasmas* **15** 055501

[60] Lake R 2013 PhD Thesis, University of Warwick, http://wrap.warwick.ac.uk/58299/

[61] Chapman I T *et al* 2010 *Nucl. Fusion* **50** 045007

[62] Menard J E *et al* 2005 *Nucl. Fusion* **45** 539

[63] Pfefferlé D, Misev C, Cooper W A and Graves J P 2014 *Nucl. Fusion* **54** 012001

[64] Menard J E *et al* 2006 *Phys. Rev. Lett.* **97** 095002

[65] Medley S S *et al* 2004 *Nucl. Fusion* **44** 1158

[66] Yakovenko Yu V, Kolesnichenko Ya I, Lutsenko V V, Burdo O S and White R B 2006 *Proc. 24th IAEA Fusion Energy Conf. (Chengdu, China, 2006)* TH/P6-6

[67] Garcia-Munoz M *et al* 2013 *Nucl. Fusion* **53** 123008

[68] Klimek I, Cecconello M and the MAST team 2016 *Proc. 43rd EPS Conf. on Plasma Physics (Leuven, Belgium, July 2016* P2.020

[69] McClements K G and Hole M J 2012 *Phys. Plasmas* **19** 072514

[70] McClements K G 2005 *Phys. Plasmas* **12** 072510

[71] McClements K G *et al* 2015 *Plasma Phys. Control. Fusion* **57** 075003

[72] Tani K *et al* 2016 *Plasma Phys. Control. Fusion* **58** 105005

[73] Pfefferlé D, Misev C, Cooper W A and Graves J P 2015 *Nucl. Fusion* **55** 012001

[74] Bortolon A *et al* 2013 *Phys. Rev. Lett.* **110** 265008

[75] Helander P, Eriksson L-G, Akers R J, Byrom C, Gimblett C G and Tournianski M R 2002 *Phys. Rev. Lett.* **89** 235002

[76] McClements K G and Turnyanskiy M R 2017 *Plasma Phys. Control. Fusion* **59** 014012

[77] Stanier A, Browning P, Gordovskyy M, McClements K G, Gryaznevich M P and Lukin V S 2013 *Phys. Plasmas* **20** 122302

[78] Embréus O, Newton S, Stahl A, Hirvijoki E1 and Fülöp T 2015 *Phys. Plasmas* **22** 052122

[79] Freethy S J *et al* 2015 *Phys. Rev. Lett.* **114** 125004

[80] Pamela S J P *et al* 2013 *Plasma Phys. Control. Fusion* **55** 095001

[81] Fredrickson E D *et al* 2016 *Proc. 43rd EPS Conf. on Plasma Physics (Leuven, Belgium, July 2016* P2.114

[82] Morris A W *et al* 2014 IEEE Trans. Plasma Sci. **42** 402

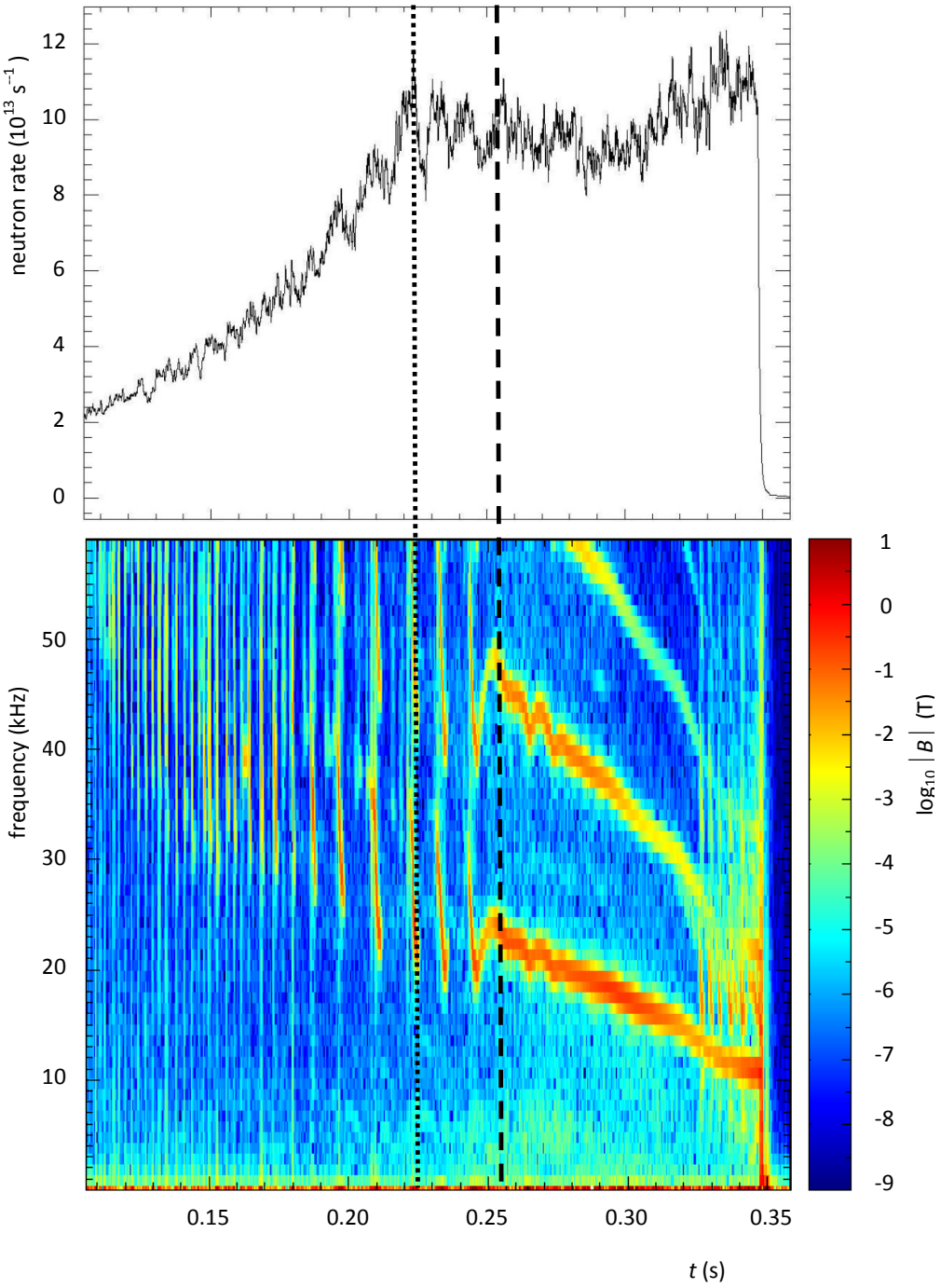

Figure 8: Total neutron rate (top) and spectrogram of magnetic fluctuations (bottom) in MAST pulse 29975. The dotted line indicates the time of excitation of a fishbone, and the dashed line indicates the time at which the fishbones were replaced with a long-lived mode.

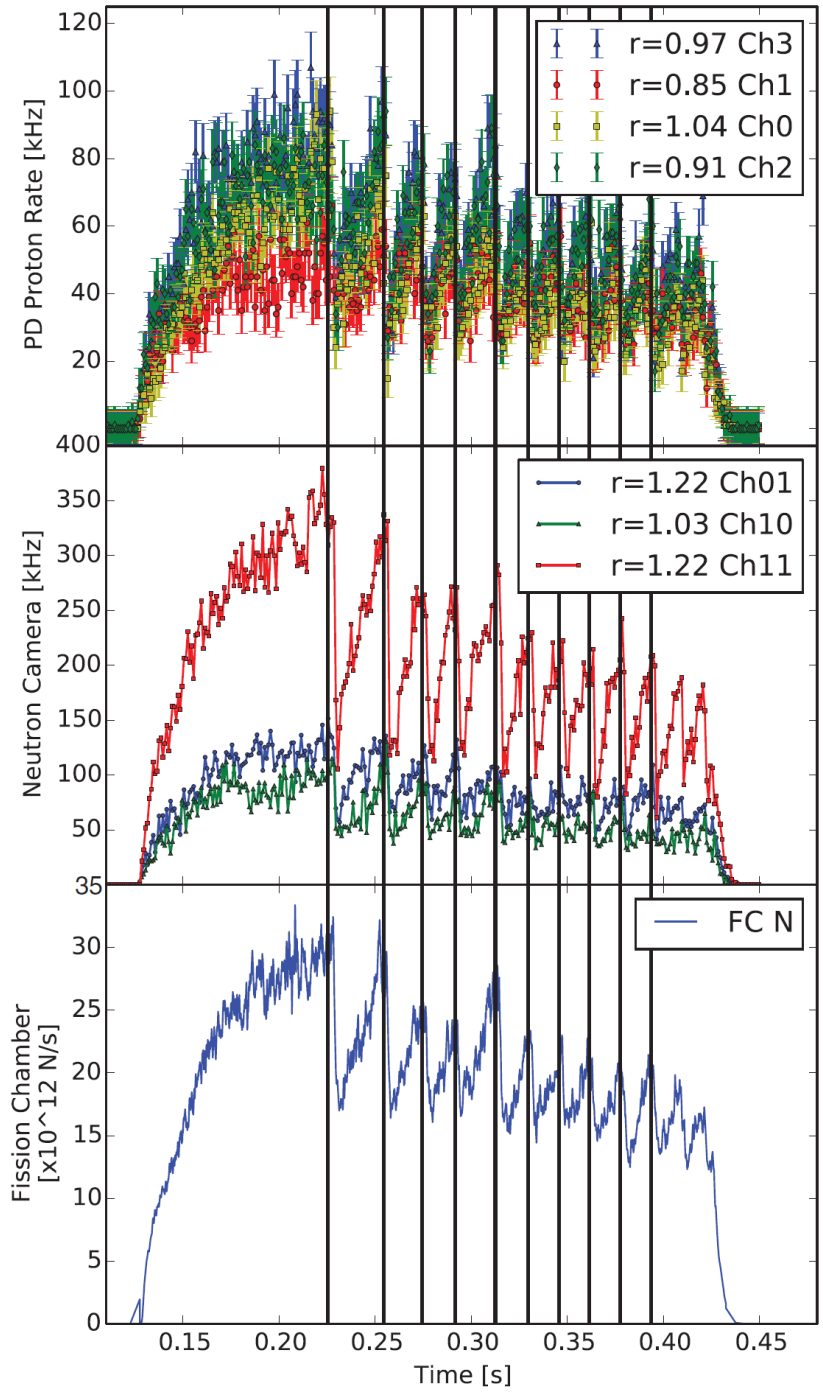

Figure 9: Temporal evolution of fusion proton fluxes (top), neutron camera fluxes (middle) and total neutron flux (bottom) in MAST pulse 29879. In the fusion proton plot the values of r are the initial major radii (in m) of protons produced in fusion reactions in the midplane, while in the neutron camera plot the values of r represent the tangency radii (again in m) of the lines-of-sight. (Reproduced from [6] with permission from American Institute of Physics.)

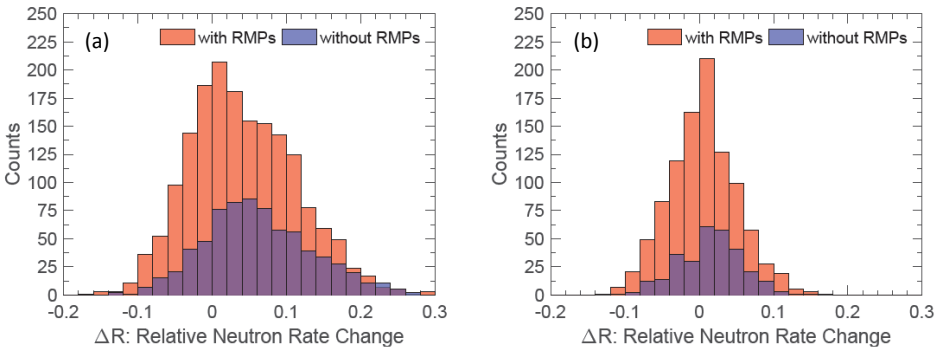

Figure 10: Distributions of relative changes in total neutron emission following ELMs in single null MAST plasmas with plasma currents of (a) 600 kA and (b) 400 kA. Positive values of ΔR correspond to a reduction in neutron flux.(Reproduced from [68].)

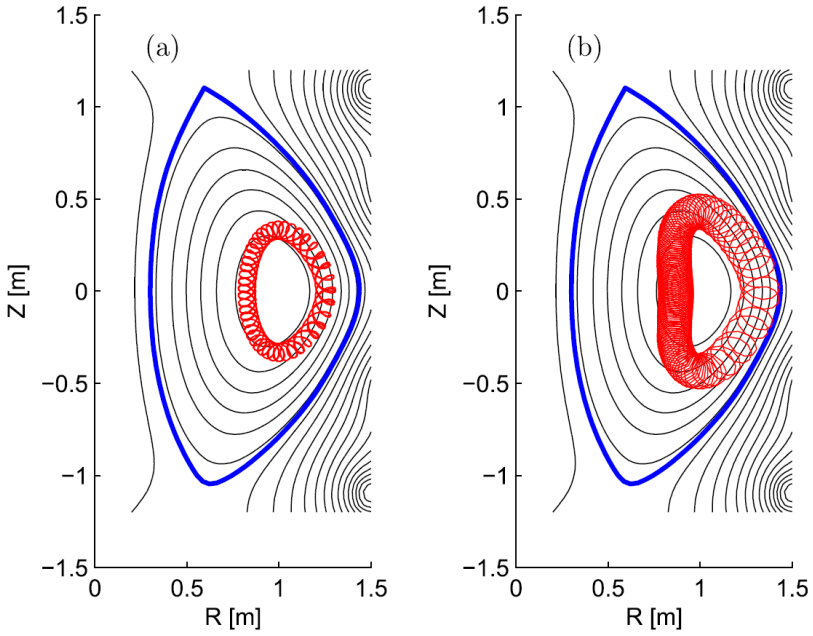

Figure 11: Projections onto the poloidal plane of energetic beam ion orbits in MAST. The ions were born at (a) $R = 0.81\,\mathrm{m}$, $Z = 0.12\,\mathrm{m}$ and (b) $R = 1.32\,\mathrm{m}$, $Z = 0.02\,\mathrm{m}$. Black curves show flux surface contours, with the last closed flux surface in blue. (Reproduced from [69] with permission from American Institute of Physics.)

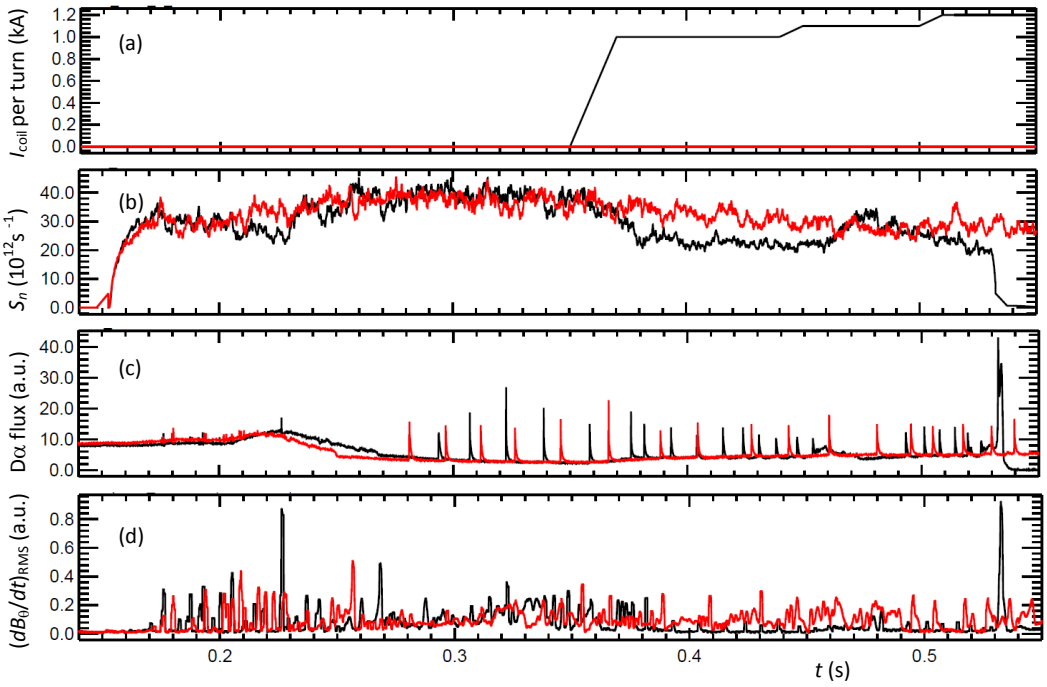

Figure 12: Time traces from MAST pulses 30086 (black) and 30090 (red) showing (a) RMP coil current per turn, (b) total neutron rate, (c) Dα emission, and (d) root mean square rate of change of poloidal magnetic field measured using Mirnov coil outside plasma. (Reproduced from [71] with permission from IOP Publishing.)

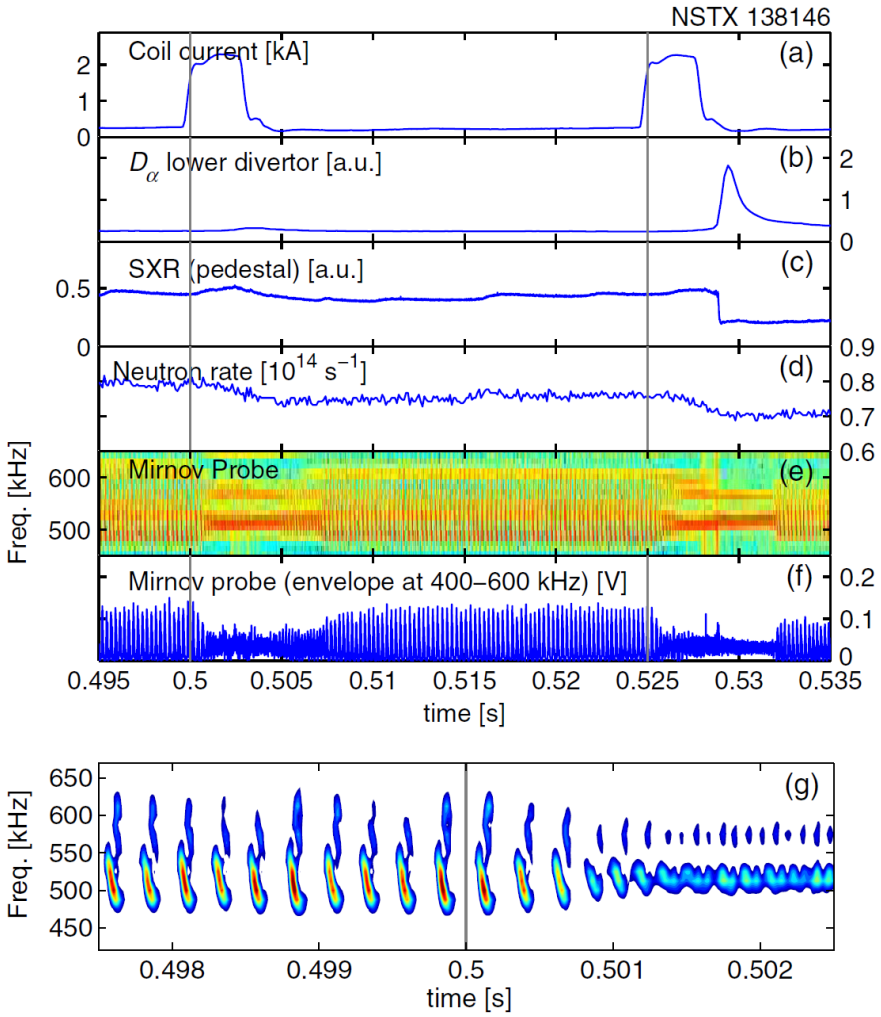

Figure 13: Time traces from NSTX pulse 138146 showing (a) RMP coil current per turn, (b) Dα emission, (c) soft X-ray emission from the pedestal region, (d) neutron rate, (e) spectrogram of high-frequency Alfvén activity, (f) magnetic coil signal, and (g) a blow up of the spectrogram immediately before and after the time (0.5 s) at which the RMP current was switched on. (Reproduced from [74]. Copyright 2013 by The American Physical Society.)

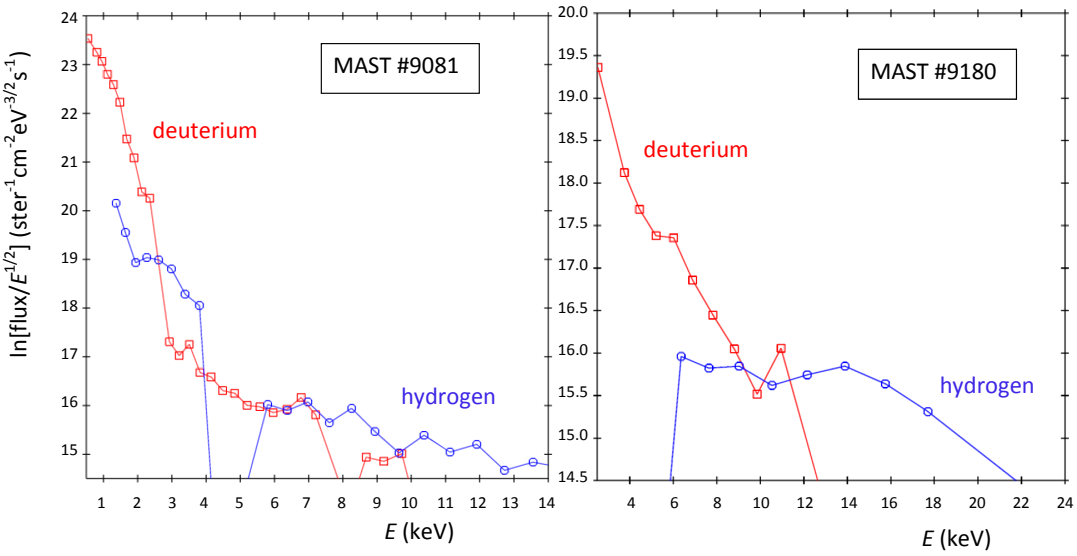

Figure 14: NPA spectra for deuterium (squares/red curves) and hydrogen (circles/blue curves) obtained during the merging-compression phases of two similar MAST pulses, 9081 (left) and 9180 (right), before the start of NBI. In each case the neutral particle fluxes were integrated in time over 8 ms.

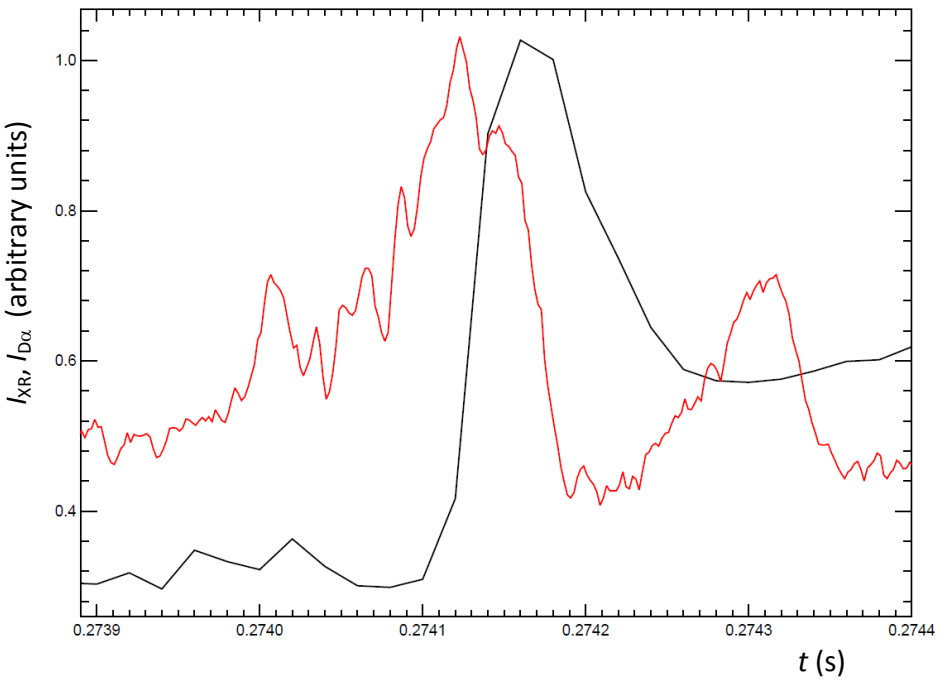

Figure 15: Evolution of soft X-ray intensity (red curve) and Dα intensity (black curve) during a typical ELM in MAST. The X-rays were detected along a line-of-sight passing through the low field side plasma edge above the midplane.

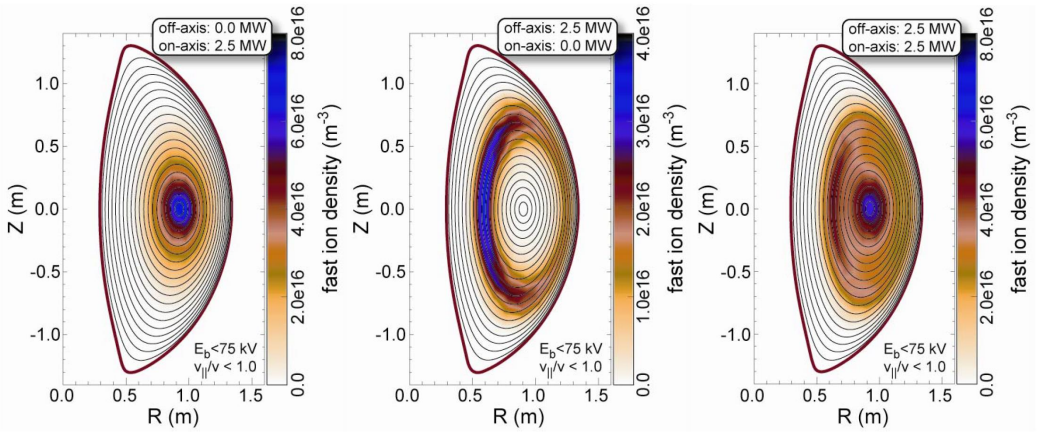

Figure 16: Predicted fast ion density profiles in MAST-Upgrade with different combinations of on-axis and off-axis neutral beam injection. (Reproduced from [82].)